JPL PUBLICATION 77-74

Dual-Spin Attitude Control for Outer Planet Missions

December 15, 1977

National Aeronautics and Space Administration

Jet Propulsion Laboratory
California Institute of Technology
Pasadena, California 91103

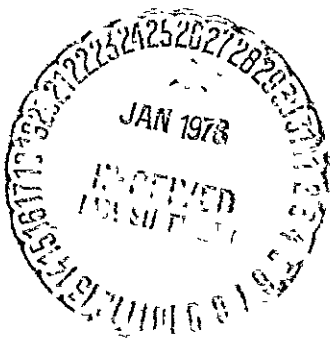

TECHNICAL REPORT STANDARD TITLE PAGE

1. Report No. JPL Pub. 77-74	2. Government Accession No.	3. Recipient's Catalog No.
4. Title and Subtitle Dual-Spin Attitude Control for Outer Planet Missions		5. Report Date December 15, 1977 6. Performing Organization Code
7. Author(s) R. S. Ward/G. J. Tauke		8. Performing Organization Report No.
9. Performing Organization Name and Address JET PROPULSION LABORATORY California Institute of Technology 4800 Oak Grove Drive Pasadena, California 91103		10. Work Unit No. 11. Contract or Grant No. NAS 7-100 13. Type of Report and Period Covered JPL Publication
12. Sponsoring Agency Name and Address NATIONAL AERONAUTICS AND SPACE ADMINISTRATION Washington, D.C. 20546		14. Sponsoring Agency Code

15. Supplementary Notes

16. Abstract

The applicability of dual-spin technology to a Jupiter Orbiter with Probe mission has been investigated. Basic mission and system level attitude control requirements were established and preliminary mechanization and control concepts developed. A comprehensive 18-degree-of-freedom digital simulation was utilized extensively to establish control laws, study dynamic interactions, and determine key sensitivities. Fundamental system/subsystem constraints have been identified, and the applicability of dual-spin technology to a Jupiter Orbiter with Probe mission has been validated.

17. Key Words (Selected by Author(s)) Spacecraft Design, Testing and Performance	18. Distribution Statement Unclassified - Unlimited		
19. Security Classif. (of this report) Unclassified	20. Security Classif. (of this page) Unclassified	21. No. of Pages 76	22. Price

HOW TO FILL OUT THE TECHNICAL REPORT STANDARD TITLE PAGE

Make items 1, 4, 5, 9, 12, and 13 agree with the corresponding information on the report cover. Use all capital letters for title (item 4). Leave items 2, 6, and 14 blank. Complete the remaining items as follows:

3. Recipient's Catalog No. Reserved for use by report recipients.

7. Author(s). Include corresponding information from the report cover. In addition, list the affiliation of an author if it differs from that of the performing organization.

8. Performing Organization Report No. Insert if performing organization wishes to assign this number.

10. Work Unit No. Use the agency-wide code (for example, 923-50-10-06-72), which uniquely identifies the work unit under which the work was authorized. Non-NASA performing organizations will leave this blank.

11. Insert the number of the contract or grant under which the report was prepared.

15. Supplementary Notes. Enter information not included elsewhere but useful, such as: Prepared in cooperation with... Translation of (or by)... Presented at conference of... To be published in...

16. Abstract. Include a brief (not to exceed 200 words) factual summary of the most significant information contained in the report. If possible, the abstract of a classified report should be unclassified. If the report contains a significant bibliography or literature survey, mention it here.

17. Key Words. Insert terms or short phrases selected by the author that identify the principal subjects covered in the report, and that are sufficiently specific and precise to be used for cataloging.

18. Distribution Statement. Enter one of the authorized statements used to denote releasability to the public or a limitation on dissemination for reasons other than security of defense information. Authorized statements are "Unclassified—Unlimited," "U. S. Government and Contractors only," "U. S. Government Agencies only," and "NASA and NASA Contractors only."

19. Security Classification (of report). NOTE: Reports carrying a security classification will require additional markings giving security and downgrading information as specified by the Security Requirements Checklist and the DoD Industrial Security Manual (DoD 5220.22-M).

20. Security Classification (of this page). NOTE: Because this page may be used in preparing announcements, bibliographies, and data banks, it should be unclassified if possible. If a classification is required, indicate separately the classification of the title and the abstract by following these items with either "(U)" for unclassified, or "(C)" or "(S)" as applicable for classified items.

21. No. of Pages. Insert the number of pages.

22. Price. Insert the price set by the Clearinghouse for Federal Scientific and Technical Information or the Government Printing Office, if known.

JPL PUBLICATION 77-74

Dual-Spin Attitude Control for Outer Planet Missions

R. S. Ward
G. J. Tauke

December 15, 1977

National Aeronautics and
Space Administration

Jet Propulsion Laboratory
California Institute of Technology
Pasadena, California 91103

Prepared Under Contract No NAS 7-100
National Aeronautics and Space Administration

PREFACE

The work described in this report was performed by the Control and Energy Conversion Division of the Jet Propulsion Laboratory.

ACKNOWLEDGMENTS

The authors wish to express appreciation to Gary Parker for his many valuable comments and suggestions on dual-spin attitude control concepts. Thanks go to Dr. Touraj Assefi for performing the preliminary JOP pointing accuracy analysis. The assistance of Lorey McGlinchey, Dr. Elbert Marsh, and Gerald Fleisher is also gratefully acknowledged.

ABSTRACT

The applicability of dual-spin technology to a Jupiter Orbiter with Probe mission has been investigated. Basic mission and system level attitude control requirements were established and preliminary mechanization and control concepts developed. A comprehensive 18-degree-of-freedom digital simulation was utilized extensively to establish control laws, study dynamic interactions, and determine key sensitivities. Fundamental system/subsystem constraints have been identified, and the applicability of dual-spin technology to a Jupiter Orbiter with Probe mission has been validated.

CONTENTS

APPENDIXES

Figures

Tables

SECTION I

INTRODUCTION

Conceptually, one of the simplest ways to achieve momentum exchange for attitude control is to allow the whole spacecraft to spin about a single axis. Naturally, this severely constrains the vehicle design and mission applications, but it is inherently stable and essentially passive. Exemplification of this technique, which is commonly referred to as simple spinners, is the Syncom series, the first synchronous communications satellites. Most missions, however, cannot be accomplished with simple spinners because all parts rotate together, and hence no oriented sensors or antennas can be employed. The next logical step in the evolution of such spacecraft is to combine an oriented platform on a spinning spacecraft. The concept retains the advantage of gyroscopic stiffness and yet permits the inertial pointing of platforms, science instruments, antennas, etc. In addition, a spinning platform is available for large field-of-view experiments such as fields and particles. Spacecraft with spinning rotors and despun platforms are called dual spinners. Many of the earth-orbiting commercial satellites launched since the early 1970s have this configuration. Such designs have typically been axisymmetric and have not included the long, flexible appendages which are commonplace on today's planetary spacecraft. The question naturally arises then: What are the implications of using a dual spinner for the exploration of the outer planets?

During FY'77, the applicability of dual-spin technology to outer planet missions was investigated under NASA RTOP 186-68-90, Dual Spin Attitude Control for Outer Planet Missions. The primary objective of the RTOP was to determine the advantages, limitations, and configuration constraints a dual-spin technology concept offered for a Jupiter Orbiter with Probe (JOP) mission. Specific objectives were to:

(1) Establish basic mission and system-level attitude control requirements.

(2) Develop preliminary control mechanization concepts and associated control laws.

(3) Investigate the effects of dynamic interactions with the control loops and determine methods for minimizing these disturbances.

(4) Determine the magnitude of, and methods to minimize, pointing errors affecting maneuver executions and instrument and high-gain antenna pointing.

(5) Determine the fundamental system/subsystem constraints.

(6) Validate the applicability of dual-spin technology to a JOP mission and be prepared for a FY'78 project start.

The investigative approach began with a survey of the dual-spin technology literature to acquire a general understanding of the fundamental principles and limitations of dual spinners, and to draw upon as much flight-proven technology as possible for the mechanization of the JOP attitude control system. (See Appendix A for bibliography.) A comprehensive 18-degree-of-freedom digital simulation was then developed and utilized extensively as the principal analytical tool. Included in the simulation were spacecraft dynamics, linear models for the sensors and actuators, conical pendulum fuel slosh models, first mode flexible booms, and the required control loops.

In the following section, a brief description of the JOP mission and spacecraft is given. Fundamental spin dynamic concepts are then reviewed, followed by detailed discussions on the attitude control mechanization concepts, and the system simulation and modeling. The results of the analysis are then presented, important findings summarized, and future considerations discussed.

SECTION II

JOP MISSION AND SPACECRAFT

A. MISSION DESCRIPTION

The principal objective of the Jupiter Orbiter with Probe mission is to conduct intensive investigations of Jupiter's atmosphere, satellites, and magnetosphere. A probe will be released into the Jovian atmosphere to measure its temperature, pressure, chemical composition, physical state, and radiation, and the aerodynamic drag on the probe. The chemical composition and physical state of the satellites will be measured and the major processes occurring on their surface identified. The magnetic properties of several satellites will also be measured to characterize the manner in which they perturb the Jovian magnetosphere. Investigations of the magnetosphere will include both time and space measurements of the absolute energy spectra and charged particle distribution. Visible light imaging equipment will be used to further examine the Jovian atmosphere and will provide high-quality pictures of the planet and satellites.

The launch of the mission is planned for early 1982, with the trip to Jupiter requiring approximately 3 years. The planned mission sequence is illustrated in Fig. 2-1.

B. SPACECRAFT DESCRIPTION

The dual-spin spacecraft configuration planned for the JOP mission is a somewhat radical departure from the three-axis-stabilized vehicles previously flown by JPL. Its principal advantage over the inertially stabilized vehicles is its capability to accommodate all classes of science instrumentation, i.e., inertial platforms for imaging and rotating platforms for fields and particles experiments. Figure 2-2 shows the configuration as assumed for this study. During the course of the study, the configuration did change several times; however, no attempt was made to track these changes, not only because it

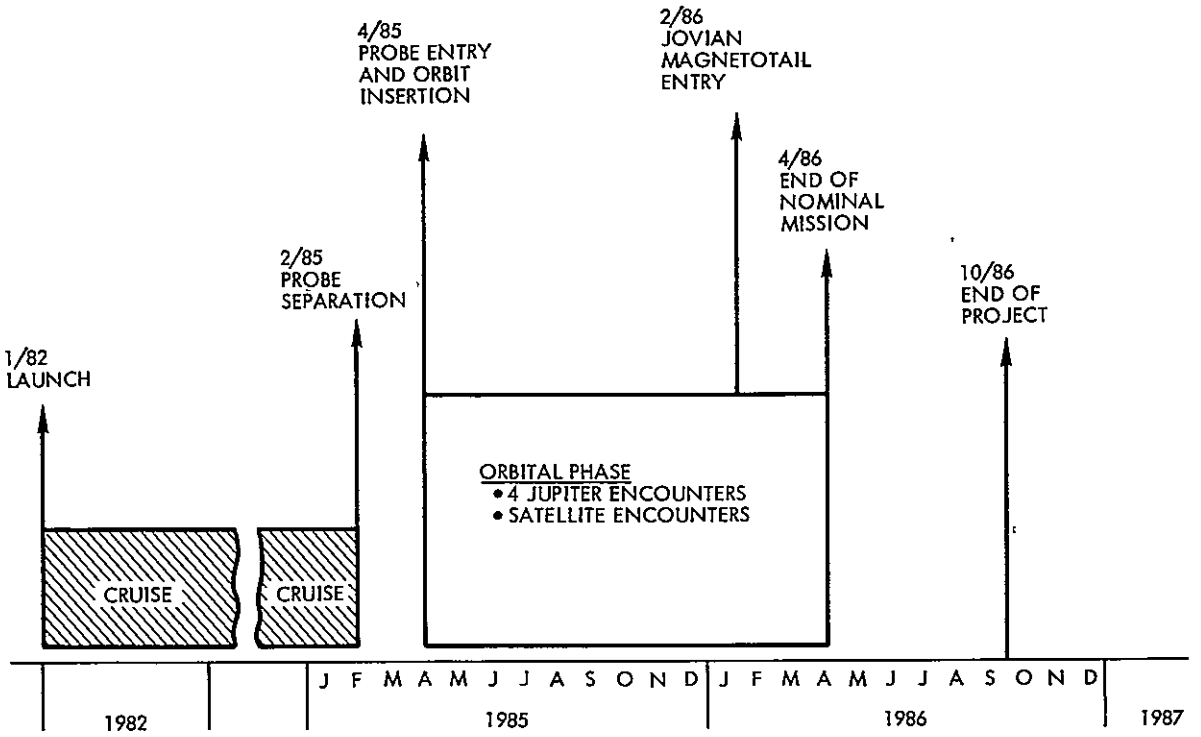

Fig. 2-1. Mission Sequence

was impractical to do so but also because of the fundamental nature of the study.

Attached to the spinning portion of the spacecraft are three deployable booms, two for the radioisotope thermoelectric generators (RTGs) and one for the fields and particles experiments. The propulsion system is a bipropellant type using MMH and N_2O_4. It is mounted on the spin section and provides all ΔV maneuvers and attitude control torques. Attached below it is the entry probe. The despin platform is attached to the spin section by means of a despin bearing/actuator assembly. The actuator provides despin and scan clock angle control torques. Mounted to the side of the despin section is the scan platform, which contains the charge-coupled device (CCD), framing camera, infrared spectrometer, and probe relay antenna. The scan platform is

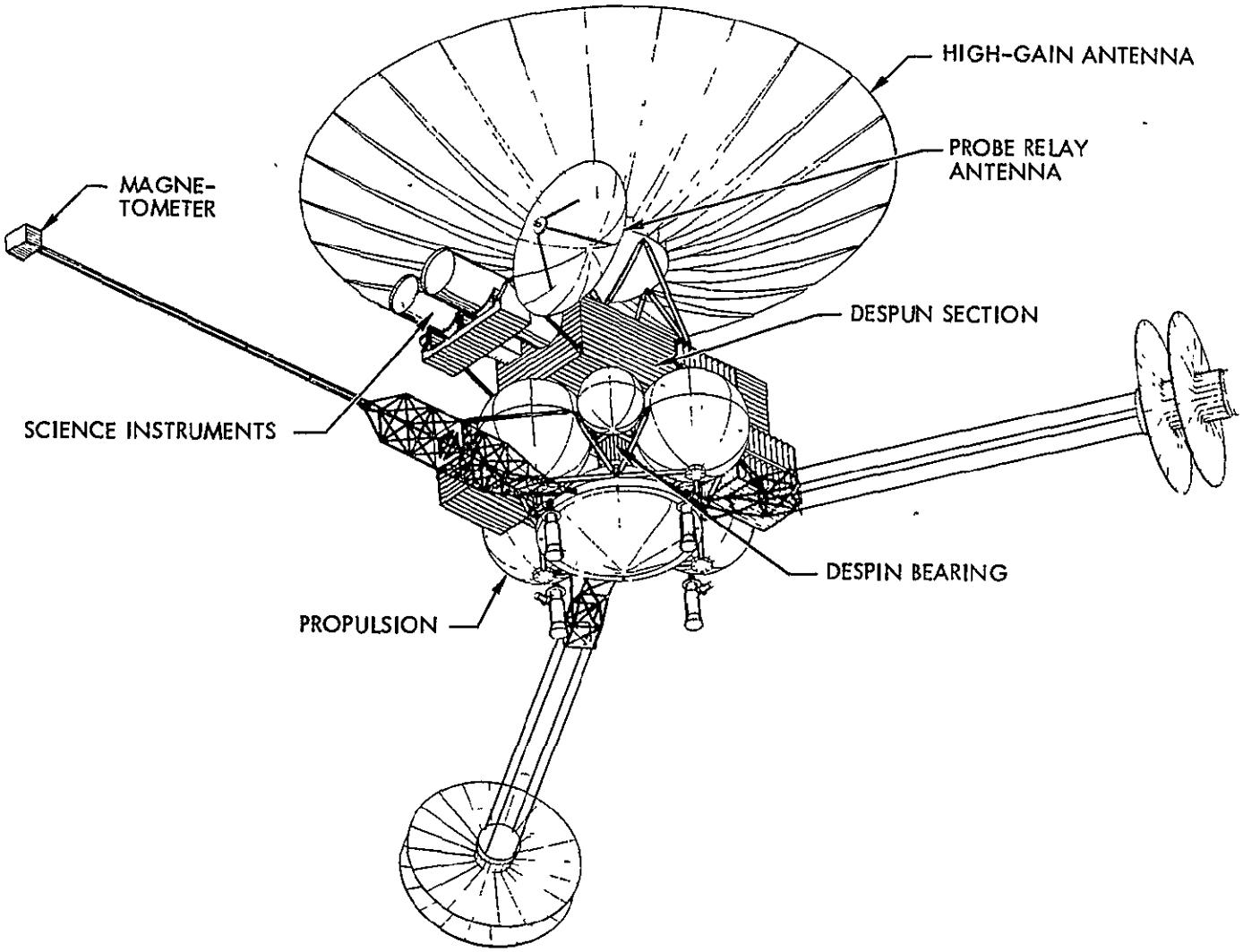

Fig. 2-2. JOP Spacecraft

free to move only in cone angle, with clock angle obtained by rotating the entire despin section. The high- and low-gain antennas used to communicate with earth are mounted on top of the despin section and aligned with the bearing axis. A summary of the mass and inertia properties is presented in Appendix B.

C. PRELIMINARY HIGH-GAIN ANTENNA AND SCAN PLATFORM ATTITUDE POINTING ACCURACIES

Pointing accuracies in both control and knowledge are considered to be a combination of bias and stability errors, and in general are mechanical, electrical, and optical in nature. The high-gain antenna (HGA) and the scan platform accuracy requirements are interpreted as those which may not be exceeded during high-rate data transmission. For the purpose of this analysis, it is assumed that the sensors will be calibrated both on the ground and in flight so that, along with the HGA and scan platform calibration, the error allocations are met. Table 2-1 summarizes the values of the pointing control and knowledge for the HGA and the scan platform. Also included are the statistical error budgets. Each error source is in general the lump sum of detailed error sources. Each column gives the appropriate 3 σ contribution, expressed in milliradians, for each lumped error source. Since the despin platform is inertial-stabilized using a 2-degree-of-freedom gyro, the contribution of some error sources, such as the allowable drift, sensors, precession, and wobble, should be smaller in the scan platform than in the HGA. The gyro drift corresponds to 1 h of operation at the rate of 0.037 deg/h. The contingencies are considered to be independent random errors; thus the root-sum square of each contingency with its corresponding pointing capability gives rise to the appropriate pointing requirement.

Table 2-1. Preliminary Dual-Spin Pointing Requirements

Error Sources	3 σ Contribution to			
	Scan Platform Pointing		High-Gain Antenna Pointing	
	Control, mrad	Knowledge, mrad	Control, mrad	Knowledge, mrad
Allowable attitude control drift (attitude control deadband)	0.35		1.40	
Star sensor	0.50	0.20	0.50	0.20
Sun sensor	0.15	0.15	0.65	0.40
Gyro drift (0.030 deg/h)	0.65	0.65		
Control and dynamics	0.15	0.15	0.15	0.15
Nutation and wobble	0.03	0.03	0.09	0.09
Gimbal	0.15	0.15		
Antenna deformation and misalignment			0.20	0.20
Total per axis (3 σ)	0.93	0.73	1.64	0.52
Total (3 σ)	1.07	0.84	1.89	0.60
Preliminary requirement	2.00	1.00	2.00	0.90[a]
Contingency	1.68	0.54	0.65	0.67

[a]Recommended requirement.

SECTION III

SPACECRAFT DYNAMICS

Consider the dual-spin spacecraft illustrated in Fig. 3-1. The asymmetric platform is attached to an axisymmetric rotor, which is centered on z and is permitted rotation about z only. The vehicle center of mass is at the origin of the coordinate system x, y, z, and I_x, I_y, I_z are the principal moments of inertia of the entire spacecraft. The angular velocity of the platform about the body-fixed principal axes is

$$\vec{\omega} = \begin{bmatrix} \omega_x \\ \omega_y \\ \omega_z \end{bmatrix} \tag{1}$$

and ω_R is the spin rate of the rotor.

Restricting the discussion to torque-free attitude motion, the Euler equations of motion become

$$\begin{aligned} I_x\dot{\omega}_x + \left[I_z^P\omega_z + I_z^R\omega_R - I_y\omega_z\right]\omega_y &= 0 \\ I_y\omega_y - \left[I_z^P\omega_z + I_z^R\omega_R - I_x\omega_z\right]\omega_x &= 0 \\ (I_z - I_z^R)\dot{\omega}_z - (I_x - I_y)\omega_x\omega_y + I_z^R\dot{\omega}_R &= 0 \end{aligned} \tag{2}$$

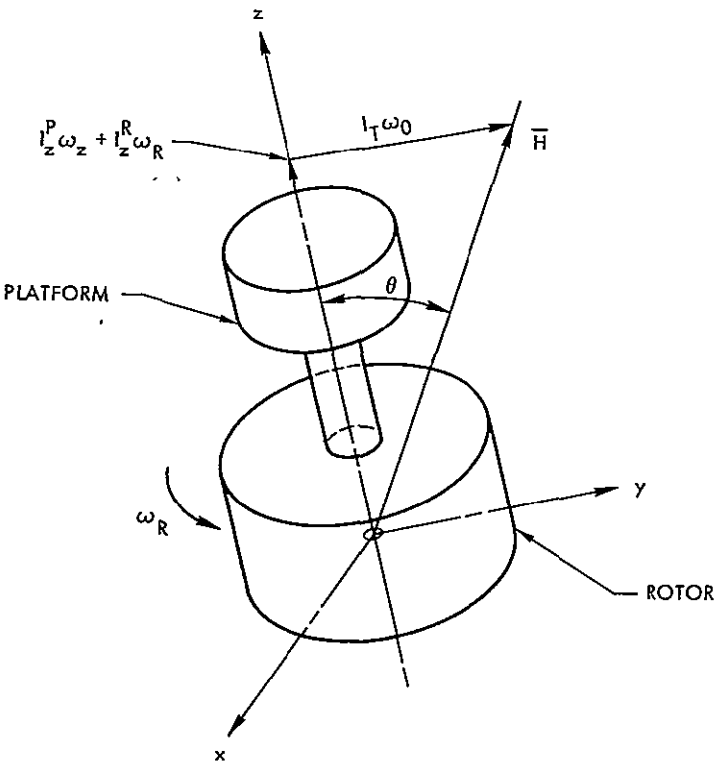

Fig. 3-1. Dual-Spin Spacecraft

where the super- and subscripts P and R designate the platform and rotor, respectively. Notice that the equations are coupled and non-linear and require several simplifying assumptions before they can readily be solved.

Assuming for the moment that the vehicle is axisymmetric and that ω_z is constant or zero, then Eq. (2) reduces to

$$\begin{aligned} \dot{\omega}_x + \lambda\omega_y &= 0 \\ \dot{\omega}_y - \lambda\omega_x &= 0 \\ I_z^R\omega_R &= 0 \end{aligned} \tag{3}$$

where

$$\lambda = \frac{I_z^P \omega_z + I_z^R \omega_R - I_T \omega_z}{I_T} \tag{4}$$

and

$$I_T = I_x = I_y$$

The rotor velocity is immediately available from Eq. (3) as

$$\omega_R = \text{constant}$$

This permits linearization of the first two equations, which then solved simultaneously yield the two transverse rates of the platform

$$\begin{aligned} \omega_x &= \omega_0 \sin(\lambda t) \\ \omega_y &= \omega_0 \cos(\lambda t) \end{aligned} \tag{5}$$

where ω_0 is the magnitude of the transverse rate in the x-y plane. The term λ is commonly referred to as the "precession rate," i.e., the rate at which the system spin vector $\bar{\omega}$ rotates about the system angular momentum vector $\bar{H}$ for an observer on the platform. Of more interest is

$$\begin{aligned} \dot{\psi} &= \lambda + \omega_z \\ \dot{\psi} &= \frac{I_z^P \omega_z + I_z^R \omega_R}{I_T} \end{aligned} \tag{6}$$

the precession rate as seen from inertial space. If $\omega_z = 0$, then Eq. (6) reduces to

$$\dot{\psi} = \frac{I_z^R}{I_T} \omega_R \tag{7}$$

Given a spacecraft with approximately equal transverse inertias, Eq. (7) provides a quick estimate of precession rate as a function of rotor speed. It is interesting to note that if

$$\frac{I_z^R}{I_T} > 1$$

the precession rate is higher than the spin rate. The angle between $\bar{\omega}$ and $\bar{H}$ during precession is referred to as the "nutation angle," which, from Fig. 3, is

$$\theta = \tan^{-1} \frac{I_T \omega_0}{I_z^P \omega_z + I_z^R \omega_R} \tag{8}$$

$$\theta = \tan^{-1} \frac{\omega_0}{\dot{\psi}}$$

Another phenomenon associated with spin dynamics that can significantly affect dual-spin vehicle performance is bearing axis wobble. Wobble occurs when the center of mass (c.m.) of the rotor does not lie on the bearing axis, i.e., the bearing axis is not coincident with the principal axis. As a result, a wobbling or coning motion of the bearing axis about the system spin vector is experienced. The angle between the bearing axis and the spin vector is referred to as the "wobble angle." If the transverse inertias are approximately equal, the wobble angle is constant in magnitude and direction for an observer on the rotor, and the rate of the coning motion is equal to the rotor spin rate ω_R. Given the above assumptions, an expression for estimating the wobble angle is

$$\phi_i = \frac{I_{iz} - mrs}{(I_z^R - I_T)} \tag{9}$$

where

i = x or y axis

I_{iz} = cross product of inertia in the x-z or y-z plane

mrs = cross product resulting from a c.m. offset

with

m = mass of offset

r = radial distance from bearing axis

s = axial distance of the offset from the system c.m.

Note that a wobble angle resulting from a c.m. offset can be effectively cancelled with a cross product of inertia, and vice versa. Further, the magnitude of the wobble angle is a function of the difference between the transverse and spin inertias; i.e., for a given c.m. offset, the wobble angle will grow as I_T approaches I_z^R.

One of the principal concerns regarding single or dual spinners is vehicle stability. Several vigorous stability arguments have been considered by Likins, Iorillo, and others, and will not be repeated here. The reader is referred to the bibliography in Appendix A for literature on the subject. The stability criterion established for dual spinners can be briefly stated as follows. If $I_z^R/I_T > 1$, then any energy dissipation on the spin and despin will have a stabilizing effect. If $I_z^R/I_T < 1$, energy dissipation on the spin section will be destabilizing, but if the energy dissipated on the despin section is greater than that on the spin section by a factor of $I_z^R/(I_T - I_z^R)$, the vehicle

will be stable. To put it another way, if the vehicle has a disc-type configuration, it is inherently stable; if it has a rod shape, the energy dissipated on the platform must exceed that on the rotor by the above factor to guarantee stability. Because of the many energy dissipating mechanisms to be found on JOP, particularly the flexible booms and fuel slosh on the spin section, it is necessary to restrict the inertia distribution to one of oblatness, i.e., disc shape. With this constraint then, any energy dissipated on the vehicle will be stabilizing, and if the energy dissipation is resonant or closely resonant with the precession rate, then appreciable nutation damping will occur, i.e., the system spin vector will be made to collapse on the angular momentum vector, thereby achieving an equilibrium spin condition with no coning motion (assuming that wobble has been eliminated). To insure that nutation damping occurs in reasonable time, a tuned passive nutation damper will be mounted on the spin or despin section.

In addition to the above criterion, if both the rotor and platform spin at different rates, the following conditions must also exist to insure stability:

$$I_z^R \omega_R + \omega_z (I_z^P - I_x) > 0$$

$$I_z^R \omega_R + \omega_z (I_z^P - I_y) > 0 \qquad (10)$$

This indicates that a minimum rotor speed is required for stability. If the platform is completely despun, then stability requires only $\overline{H} > 0$.

SECTION IV

JOP ATTITUDE CONTROL AND MECHANIZATION CONCEPTS

Spacecraft attitude control is based on the tendency of the angular momentum of the spinning section to stabilize the spin axis in inertial space. Directional changes of the angular momentum will occur only if momentum is added to system by external disturbance forces. If the stored momentum is large relative to the integrated effects of the disturbance forces, the directional displacement of the bearing axis will be small, even over a period of days. To cancel this directional drift or to change the attitude of the spacecraft for earth track or commanded turns, small bipropellant thrusters are used. Position information for these maneuvers is available from a biasable digital sun sensor or a two-axis star scanner which is used principally for spin rate control. To insure stability, the moment of inertia of the spin section about the spin axis is made larger than any transverse axis moment of inertia of the composite vehicle. In order to achieve a steady-state spin condition with no coning motion, a nutation damper is mounted on the spin section to force the spin vector to converge on the angular momentum vector.

Inexact ground balancing and uneven propellant depletion can produce a wobbling motion of the bearing axis. This motion can be greatly reduced by vernier control of the spacecraft inertias. Specifically, the RTG booms are moved up or down parallel to the bearing axis to produce cross products of inertia that effectively cancel the wobble caused by c.m. offsets or cross products of inertia.

Cone orientation of the scan platform is accomplished by a single degree of articulation relative to the despun section; clock orientation is obtained by rotating the despun section relative to the spin section. Scan platform rate and position information is provided by a two-axis tuned rotor gyro and relative position encoders.

The controller consists of redundant microprocessors with appropriate special-purpose input/output (I/O) capability. Two attitude control data bases are provided which allow the computers to communicate through remote terminals with elements of the subsystem on the despun section.

A block diagram of the JOP attitude and articulation control system (AACS) appears in Fig. 4-1.

A. SPIN CONTROL

The spin rate of the spacecraft is maintained by several bipropellant thrusters that provide torque about the spin axis as required to keep the spin rate within a desired spin rate deadband. Tight control of the spin rate is not required, and the deadband size can be ±5 - 10% of the nominally selected spin rate. Accurate knowledge of the spin rate is important, however, since the attitude control gains are a function of the angular momentum of the system. The fields and particles experiments also require accurate spin rate determination to achieve 0.1-deg position accuracy. The following factors influence the nominal spin rate selection:

(1) Resistance to disturbance torques decreases with decreasing spin rate (attitude correction frequency increase).

(2) Life of rotating components (bearings, brushes, sliprings) decreases with increasing spin rate.

(3) Propellant requirements for a given attitude correction or maneuver increase with increasing spin rate.

(4) Bearing motor torque availability decreases due to back electromotive force (BEMF) as spin rate increases.

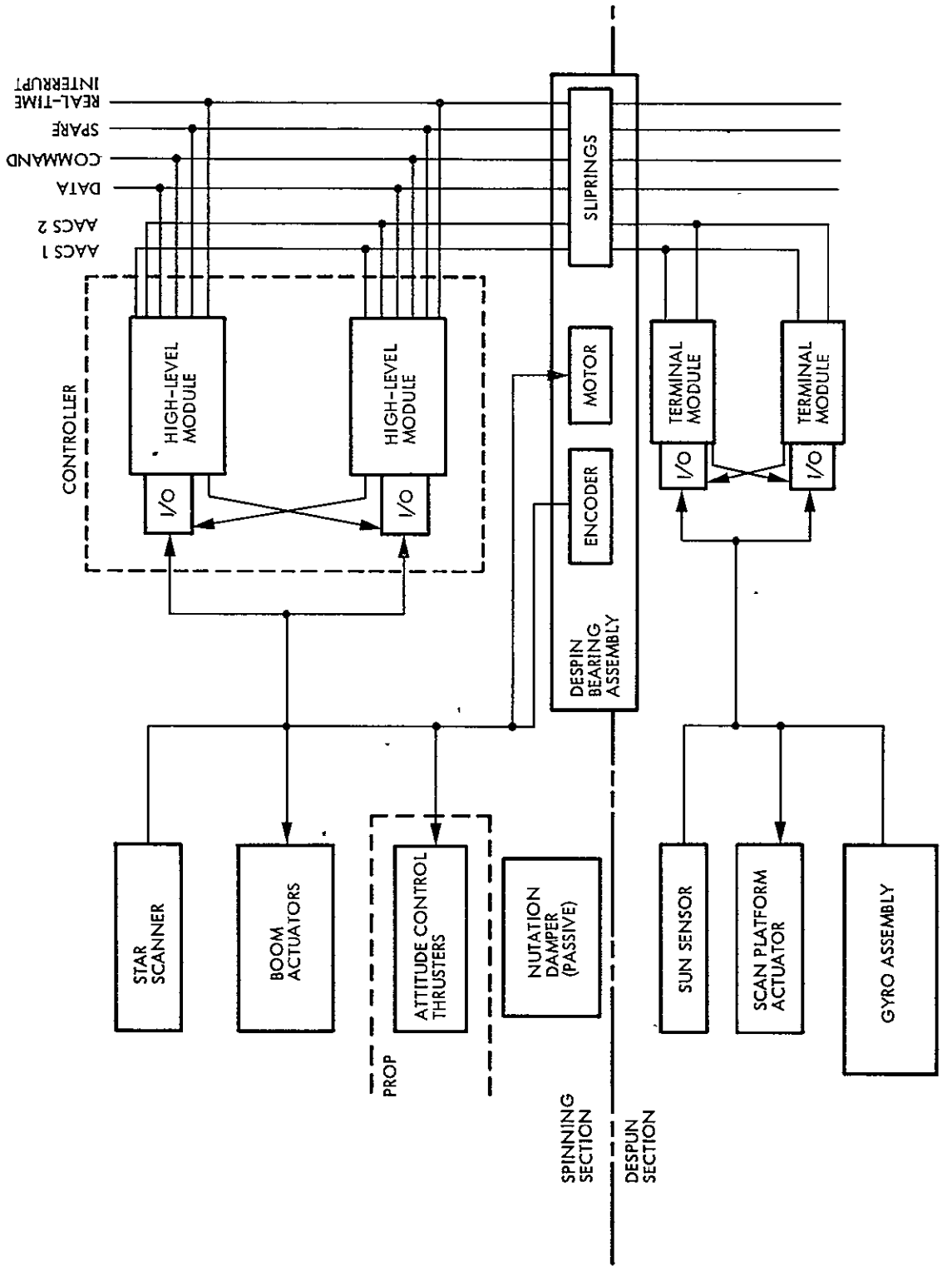

Fig. 4-1. Attitude and Articulation Control Subsystem

(5) Required minimum rocket pulse time is relaxed with increasing spin rate.

The selection for the JOP nominal spin rate is determined principally by the fields and particles experiments and is expected to be in the range of 5-10 rpm.

A block diagram of the spin rate control loop is shown in Fig. 4-2. The sensor for this loop is a star scanner, a device that provides an electronic pulse when a star sweeps across its field of view. The optical input can take several forms: a single slit, parallel slits, V-slits, or chevron pattern. Nonparallel dual-slit star scanners can provide attitude information (1) about the spin axis and (2) of the spin axis, which can be used in lieu of or as a backup to the sun sensor attitude information. Given the time between scanner outputs, the spin rate of the spacecraft can be calculated. This is held constant until the next rate calculation and is compared to the commanded spin rate to form the spin rate error. If the error signal exceeds the desired deadband, it is multiplied by the gain $K_S = \hat{I}_R/\tau$ ($\hat{I}_R$ is the estimated spin inertia and τ is thruster torque) to determine the thruster on time, Δt, required to bring the spin rate back to the middle of the deadband. How accurately this is done depends on the accuracy of $\hat{I}_R$, whose magnitude decreases as the mission progresses. This parameter may be periodically updated by ground command or may be calculated on board. Another option is to fix its value at I_R minimum, which will always result in a Δt less than or equal to what is required to achieve the middle of the deadband; this Δt will never burn excess fuel and accuracy can only improve with mission life ($I_R \rightarrow I_{Rmin}$). Since actual spin rate is not critical, only its knowledge, the use of I_{Rmin} to determine K_S should prove to be satisfactory.

B. DESPIN/SCAN CLOCK ANGLE CONTROL

The despin/scan clock angle controller is responsible for despinning and positioning (clock angle control) of the despin section.

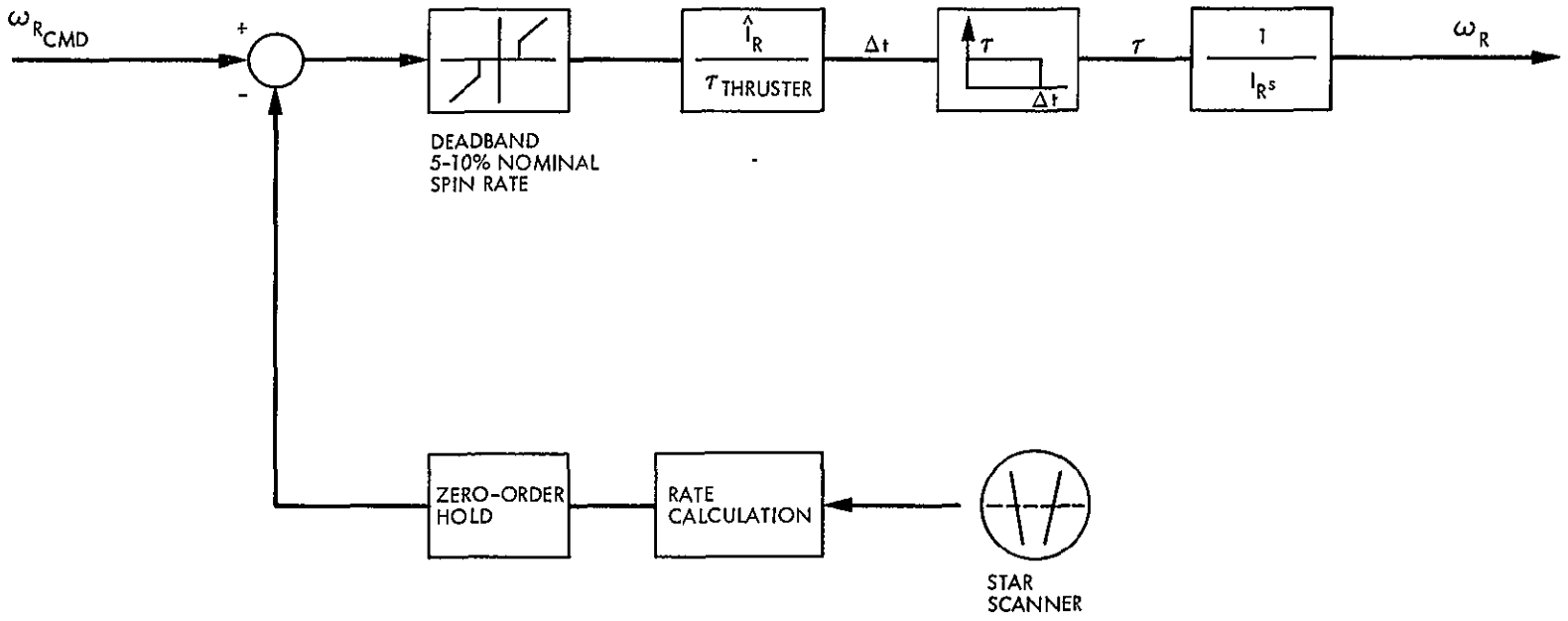

Fig. 4-2. Spin Rate Control Loop

Three sensors are used: a star scanner, which provides the inertial reference for clock; a two-axis tuned rotor gyro mounted on the scan platform, which provides clock rate and position between star scans; and a position encoder between the spin and despin sections.

To keep the despin platform fixed in inertial space, the relative position between the spin and despin section is checked with each star scan and an appropriate error signal developed to drive the despin motor to reposition or despin the platform. Since the star scanner output is available only periodically (once every 12 s using one star and an ω_R = 5 rpm), the bandwidth (BW) of this loop at best (3 stars at 10 rpm, BW $\leq$ 1 Hz) is marginal to meet the clock jitter requirements of 9 μrad. Hence, the despin loop is supplemented with the gyro during scan pointing to continuously provide platform rate and position between star scans. The position is updated with each star scan to compensate for gyro drift. Use of the scan-mounted gyro to provide the despin platform rate is not as straightforward as it first appears. Whenever the scan platform is pointing out of the x-y plane, the sensor axis and control axis are no longer colinear; hence a transformation of the control information is required (Fig. 4-3). As the platform approaches 90 deg, a gimbal lock condition is encountered. Complete operation of the despin/scan clock angle controller is illustrated in Fig. 4-4. The control law is proportional-plus-integral control, integral control being required to offset despin bearing friction.

C. SCAN CONE ANGLE CONTROL

The cone servo loop is similar to that of the clock. The scan platform is gimbaled about its c.m. in cone only and is driven by a brushless dc torquer motor. The desired cone angle is set using a high-resolution encoder. Again, proportional-plus-integral control is used, with cone rate and position being measured directly by the tuned rotor gyro. Ideally, since the scan platform is mounted about its c.m., no control effort is required to accomplish scan pointing in the presence

Fig. 4-3. Scan Platform Control Axes

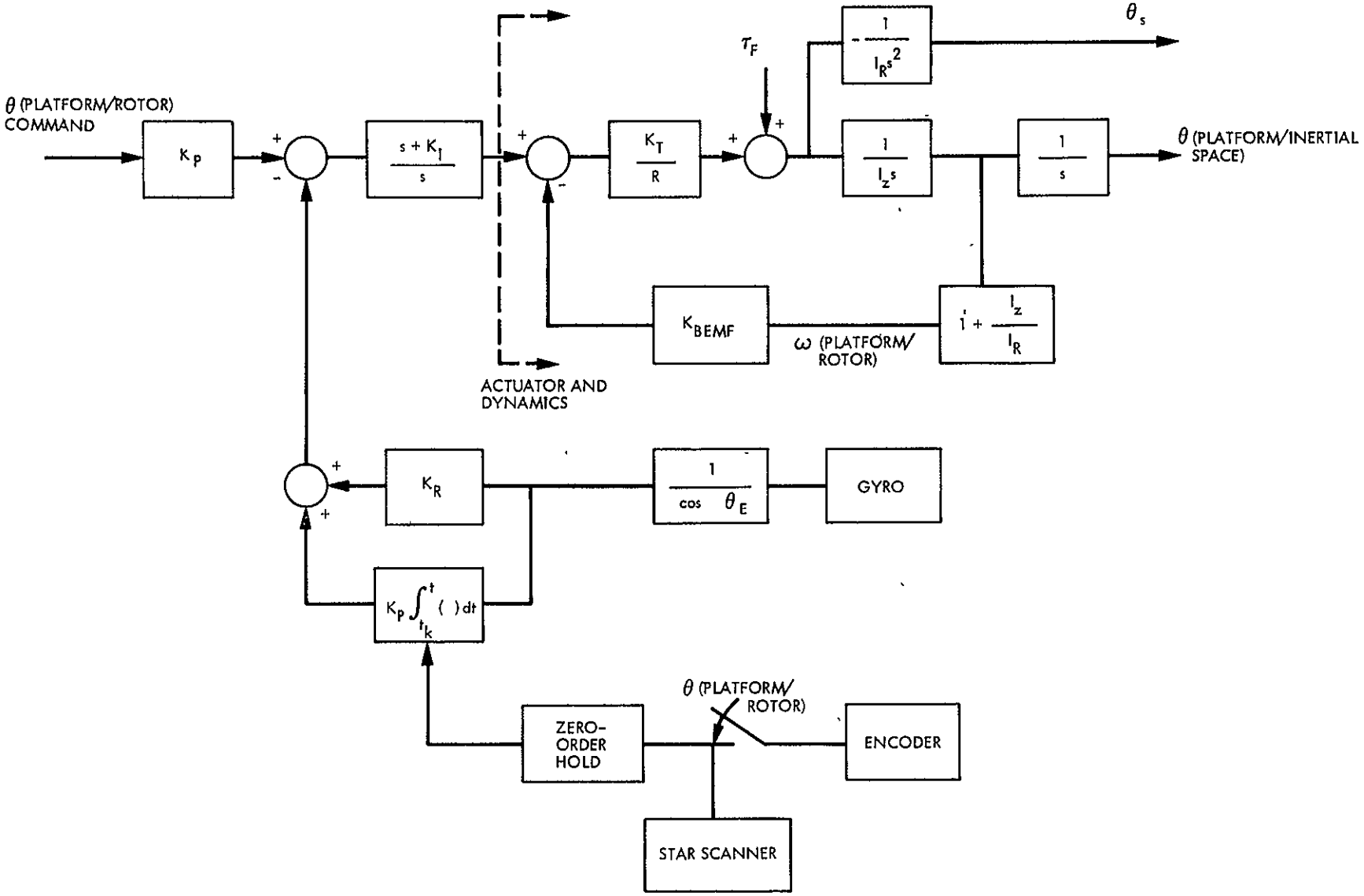

Fig. 4-4. Despin/Scan Clock Control Loop

of vehicle motion; however, because of bearing torque, cable torque, and other nonlinearities, some control effort is required, even in the absence of pointing error. Thus the requirement for integral compensation. The block diagram for the loop is presented in Fig. 4-5.

D. HIGH-GAIN ANTENNA POINTING AND COMMANDED TURNS

The high-gain antenna is a 5-m furable dish antenna rigidly mounted on the despin platform and aligned with the bearing axis. During the cruise and orbital portions of the mission, the bearing axis, and hence the HGA is pointed at the earth. HGA pointing, then, is the process of aligning the bearing axis on the earthline using attitude information from biasable digital sun sensors or a two-axis star scanner. Assume for the moment that the spacecraft is in a quiescent state (negligible precession and wobble) and pointed off the earthline at some angle greater than the HGA deadband. The HGA pointing problem is defined as follows: Align the system spin vector $\bar{\omega}_R$ and angular momentum vector $\bar{H}$ on the earthline in reasonable time using minimum propellant. Recall that whenever a spinning body experiences a transverse torque, $\bar{H}$ will move off $\bar{\omega}_R$ in the direction of the torque, and $\bar{\omega}_R$ will then precess around $\bar{H}$. Also recall that $\bar{\omega}_R$ can be made to collapse on $\bar{H}$ with a nutation damper. Thus, one strategy for accomplishing HGA pointing is to move $\bar{H}$ back on the earthline using thrusters and wait for the precession to dampen. This method has the advantages of being simple, requiring few computations, and using close to minimum gas. It will take, however, on the order of 15-30 min for $\bar{\omega}_R$ to converge for a reasonable size nutation damper, and the size of the precession cone will be larger than the HGA deadband for some portion of that time. The technique is illustrated in Fig. 4-6.

Another common method for accomplishing precession maneuvers is to rotate $\bar{H}$ halfway to the earthline, wait for $\bar{\omega}_R$ to precess 180 deg, and then move $\bar{H}$ onto $\bar{\omega}_R$. The advantage here is that the maneuver takes only half a spin period and, once completed, no precession is present. It does require that once $\bar{\omega}_R$ has precessed 180 deg, a thruster on the spin section be in a proper position to move $\bar{H}$ onto $\bar{\omega}_R$. This will not occur

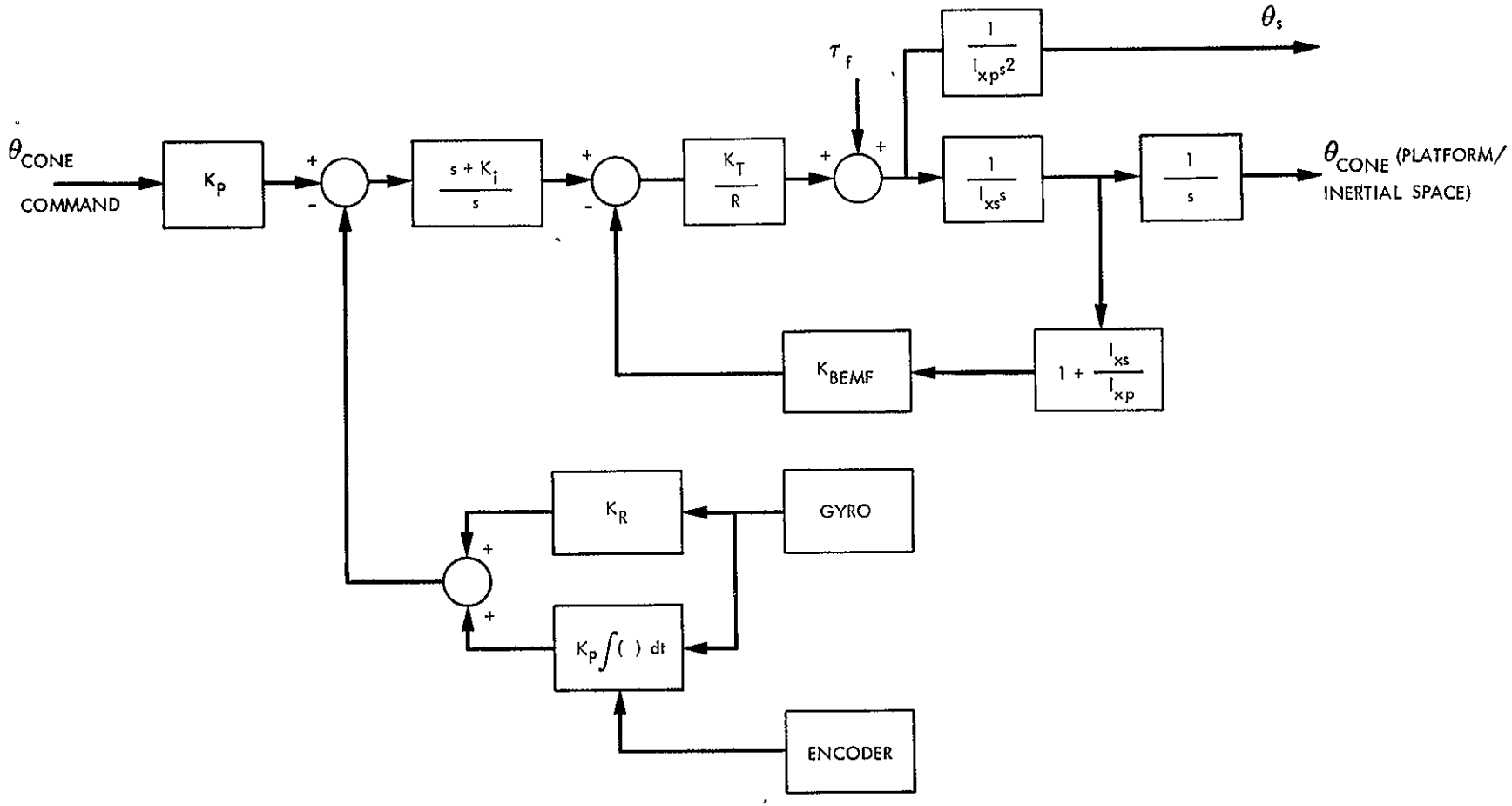

Fig. 4-5. Scan Cone Control Loop

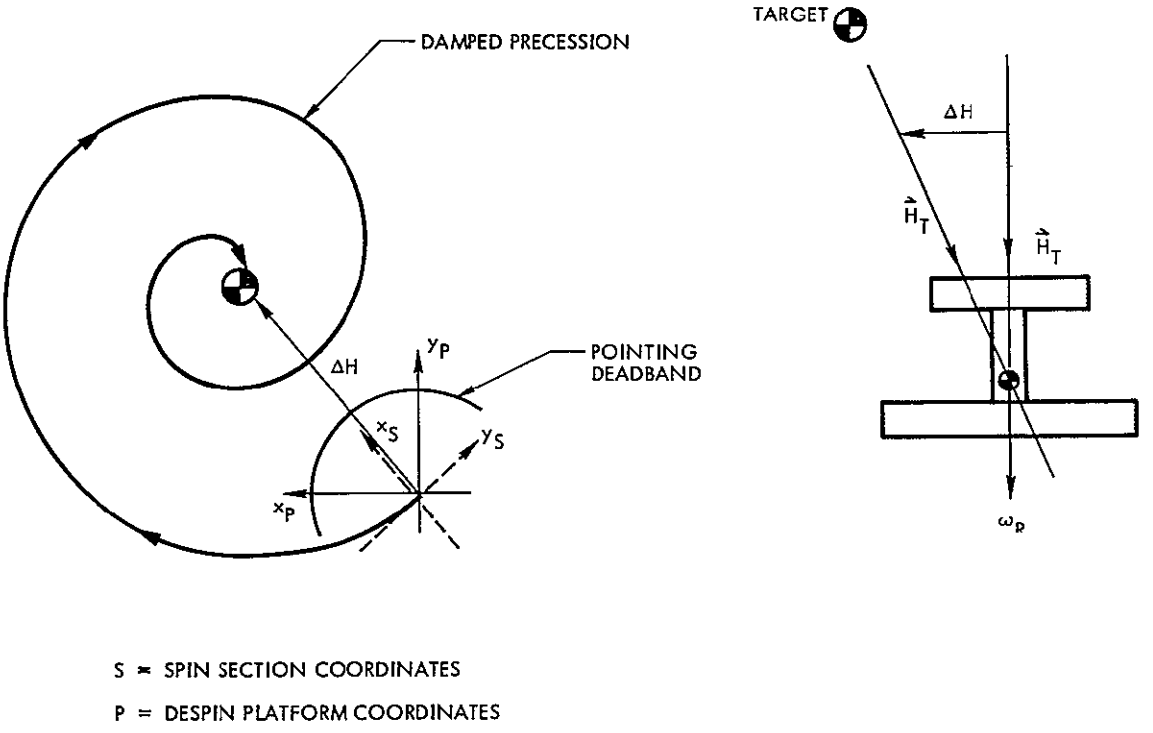

Fig. 4-6. One-Burn Scheme

unless the precession rate is a particular integer multiple of the spin rate, assuming a symmetric thruster configuration; what that integer is depends on the thruster configuration. It will generally be necessary to wait several precession revolutions until a thruster is available at the right position; i.e., the bearing axis must precess through the angle 180 + 360n deg, where n is the number of additional precession revolutions required before a thruster is in the correct position. For our case at $\bar{\omega}_R$ = 5 rpm, n = 10. That is, the bearing axis must precess 10½ revolutions before a thruster is available; the corresponding time is approximately 94 s. If the amount of nutation damping during this period is significant, it will have to be taken into account when calculating the second thruster burn time; however, the time constant of the damper is expected to be in the range of 5 to 10 min, so the amount of nutation damping occurring in the first couple of minutes can mostly likely be neglected in the burn time calculation. The advantages of this scheme over the one-burn scheme are that it will be 15 to 30 times

faster, depending on the size of the nutation damper; no precession is present at the end of the maneuver; and it is closer to gas optional. (The amount of gas needed for a maneuver is a function of the amount of damping required, among other things.) On the other hand, it is more computationally complex for high rates of nutation damping, and it requires an accurate estimate of the precession rate. Any error in the estimate of the precession rate will decrease the knowledge of where the bearing axis is on the precession cone, and the knowledge will decrease with each precession revolution of the bearing axis; i.e., the error is additive with each precession revolution. Although the two-burn scheme is considerably faster than the one-burn, it is far from being fast. This scheme is shown in Fig. 4-7.

A third method, which is both time and gas optional and simple to execute, is the three-burn scheme. In this scheme, no additional waiting for thruster alignment is required. Assume for the moment that we have four thrusters 90 deg apart and that we start a precession

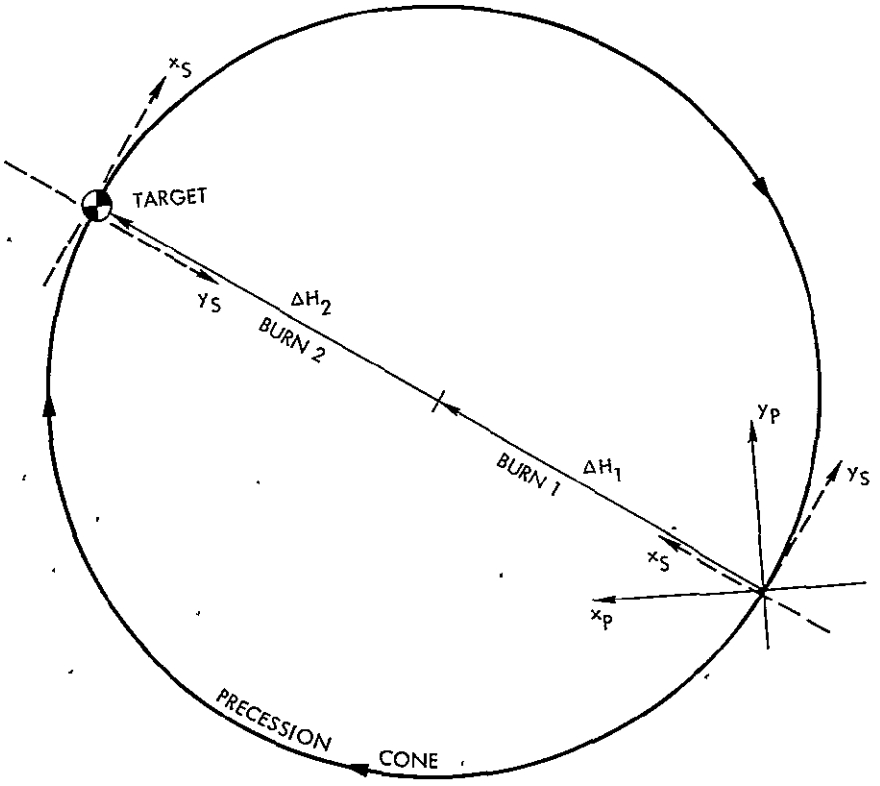

Fig. 4-7. Two-Burn Scheme

maneuver when thruster 1 is pointed in the direction of the earthline. As before, the bearing axis will start to precess around $\overline{H}$ after the firing. When the spin section has rotated 90 deg, thruster 2 is pointed in the direction of the earthline and fired. $\overline{H}$ is moved closer to the target, and the precession continues. After the spin section has rotated another 90 deg, thruster 3 is pointed at the target, and the bearing axis is on the target. Hence, when thruster 3 is fired at this time, $\overline{H}$ moves onto the target along with the bearing axis, and the maneuver is completed with no precession present. The execution time is one-half the spin period. For ω_R = 5 rpm, the time required is only 6 s. The technique is illustrated in Fig. 4-8. This scheme does require a certain thruster resolution to be viable for HGA pointing; i.e., the angle resulting from a minimum thruster burn must be something less the one-third the HGA pointing deadband radius. The amount of resolution is primarily a function of the spin rate and the length of the thruster moment arms. The three-burn scheme can be extended to an n-burn scheme.

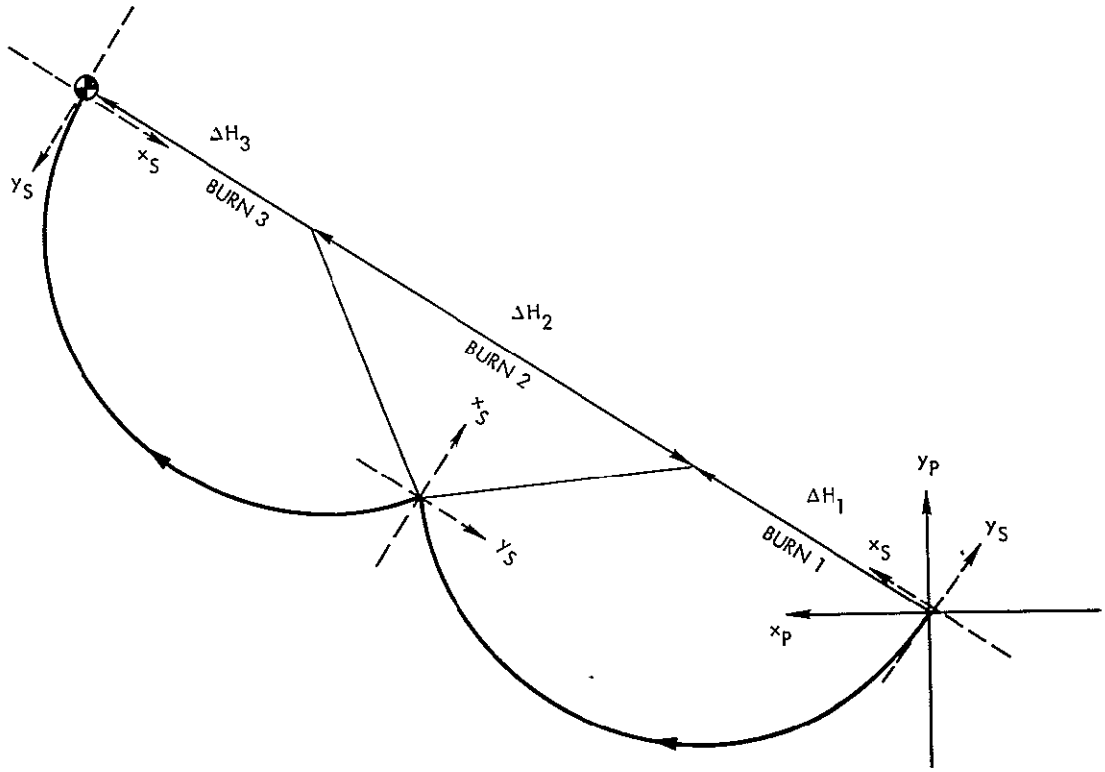

Fig. 4-8. Three-Burn Scheme

In this method, the precession is simply ignored, and a thruster is fired with a constant burn time every time it is aligned in the direction of the target. The nutation angle will build up and then decrease in a cyclic fashion, and nutation damping will be required at the end of the maneuver if it does not occur at a nutation minimum. This scheme will not be viable for HGA pointing because the required thruster resolution becomes excessively high.

Several schemes have been presented for performing attitude corrections or achieving HGA pointing. It is appropriate at this point to consider commanded turns of the spacecraft. A commanded turn is nothing more than a series of precession maneuvers like the ones described above. The size of a precession maneuver is limited by the angle through which the thruster can burn. Maximum $\overline{H}$ deviation can be obtained by burning through 180 deg, but there is a cosine efficiency loss, and hence it is desirable to keep the burn angle as small as possible. If the burn angle is restricted to ±5 deg, the time required to accomplish a command turn using the one- or two-burn scheme becomes unreasonable. The three- and n-burn schemes, however, lend themselves very nicely to command turns. Several turns are planned during the mission that require the spacecraft to move off the earthline and break high-data-rate earth communications. These turns can be performed either open or closed loop. Open loop is accomplished by precalculating all thruster burns and then executing them at the proper time and sequence. To do a closed-loop turn, the cone input axis of the gyro on the scan platform is rotated orthogonal to the direction of the turn and is then used to provide rate and position for feedback control. The tradeoffs between the two schemes have not yet been determined.

E. WOBBLE CONTROL

Wobble motion resulting from c.m. offsets and their corresponding crossproducts of inertia are a source of attitude errors affecting HGA pointing and angular position knowledge of the fields and particles

experiments. Recall from Eq. (9) that a c.m. offset is effectively a cross product of inertia and vice versa. Wobble angle can be significantly reduced by moving a mass on the spin section in such way as to create a cross product of inertia equal and opposite to that causing the wobble. Efficient utilization of spacecraft mass dicates that the mass used to effect the corrective offset be an already existing one. Preliminary calculations indicate that the weight of a dedicated wobble mass would be excessive, particularly if this mass were near the center of the spacecraft. The prime candidates for the wobble mass are the two RTGs. They are massive and located over 3 m radially from the bearing axis. Sufficient cross products of inertia can be obtained by adjusting the angle of the RTG booms in a plane extending through the bearing axis. Good wobble control about both transverse axes can be achieved if the booms are separated around 120 deg in the x-y plane. A c.m. offset of 1 cm off the bearing axis will require a boom angle movement of about 0.5 deg.

The method or technique used to determine wobble angle, which is constant as seen by an observer on the spin section, depends on the source of attitude information. If platform-mounted sun sensors are used, their outputs must first be transformed to the spin coordinates before the wobble angle can be calculated. The CORDIC transformation algorithm is the most computationally convenient method of performing this transformation, since generation of sines and cosines is not required. If spacecraft attitude information is obtained from a sensor on the spin section, such as a two-axis star scanner, a coordinate transformation is not required, and the wobble angle can be calculated directly from the attitude information. Given the wobble angle, the required boom angle can then be calculated. The boom actuators will most likely be geared-down stepper motors with some type of locking mechanism. Initial wobble correction will be required shortly after separation; thereafter, it will be required only after large quantities of mass have been expelled, i.e., after many trajectory correction maneuvers, probe release, or orbit insertion or corrections.

SECTION V

SYSTEM MODELING AND SIMULATION

Modeling of the spacecraft dynamics was greatly simplified by the availability of dynamic simulation subroutines for systems of hinge-connected rigid bodies. This family of subroutines commonly referred to as MBDY (multi-body) subroutines was developed by Fleischer and Likins at JPL (see Ref. 43 in Appendix A). The specific subroutine selected for this study was MBDYM, a nonlinear rigid-body MBDY that accommodates rotational motion. The subroutine determines the angular accelerations of each body in a collection of bodies configured in a topological tree with no closed loops. Connections between bodies are permitted rotational motion only; no translation between contiguous bodies is permitted. Data passed to the subroutine include: number of hinges, degrees of freedom and direction of freedom for each hinge, distances from the hinges to the c.m. of attaching bodies, mass and inertia properties of each body, torques about the hinges, forces acting on each body, and finally, the positions and rates of each body. Given the relative angular accelerations between the bodies, the rates and positions of each body can be determined through integration. Integration was accomplished using the Continuous System Simulation Language (CSSL), a simulation package utilizing a variable step integration subroutine.

A. SPACECRAFT

The complete 18-degree-of-freedom (DOF) model, shown in Fig. 5-1, is composed of the following rigid bodies:

(1) Despin section (0 DOF)

(2) Scan platform (1 DOF)

(3) Pendulous nutation damper (2 DOF)

(4) Fuel slosh models (4 tanks, 2 DOF each)

(5) Magnetometer boom (2 DOF)

(6) RTG booms (2 booms, 2 DOF each)

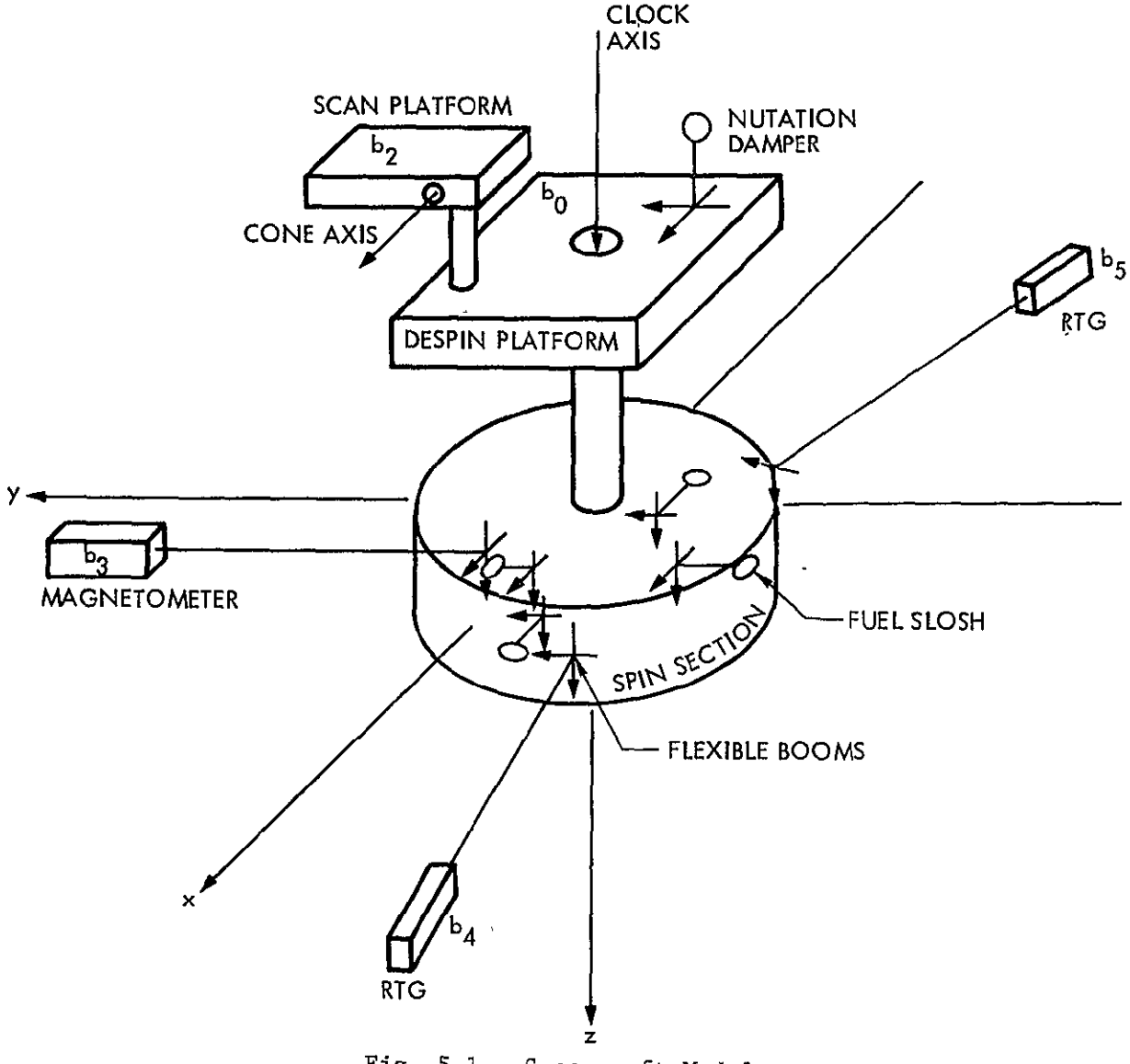

Fig. 5-1. Spacecraft Model

The two RTGs were modeled as 30-kg point masses mounted on 3.175-m-long massless booms. The magnetometer was 22.5 kg, with a boom length of 4.4 m. The fundamental mode of flexibility for 2 degrees of freedom was also included. The undamped natural frequency for the RTG booms was 1 Hz and for the magnetometer boom 0.5 Hz. All booms were mounted 0.5 m from the bearing axis and had damping ratios of 0.005.

B. SENSORS AND ACTUATORS

The scan and bearing actuators were modeled as linear brushless dc torque motors, with peak torque capabilities of 0.21 and 2.8 Nm, respectively. Candidate motors were selected from the Magnetics Technologies dc motor catalog; their properties are summarized in Table 5-1. Since the relative rate between the spin and despin sections never changes sign, the despin bearing friction was modeled as coulomb friction with a value of 0.54 Nm. Scan platform bearing friction for this study was assumed to be zero. It is recommended that a nonlinear Dahl model be incorporated for future work. All sensor models were linear and did not include sensor dynamics or noise.

C. FUEL SLOSH

One of the early concerns at the onset of this study was the effect of fuel slosh on vehicle performance. Fuel slosh represents energy dissipation on the spin section, and, as discussed earlier, this could be destabilizing if $I_R/I_T < 1$. On the other hand, if $I_R/I_T > 1$, it can be a source of nutation damping if the frequencies of fuel slosh are near the precession rate. To date, a significant amount of work has been done on the development of lateral fuel slosh models, i.e., models that describe liquid motion occurring primarily in response to translational or pitching motions of a nonrotating tank. Some work has even been done on tanks spinning through their center, but very little is to be found on fuel tanks spinning off center, which is the case here. Most investigators concerned about fuel slosh on dual spinners have resorted to using lateral models for lack of anything better.

Table 5-1. Scan Clock and Cone Actuator Characteristics

Actuator / Motor Parameter	Cone MT 2780-045-139[a]	Clock MT 5125C-110-123
Peak torque, Nm	0.212	2.82
Motor torque constant, Nm/A	0.107	1.172
Winding resistance, Ω	13.9	11.6
BEMF constant, V-s	0.107	1.16

[a]Magnetics Technologies.

Although this does have a major shortcoming, a lateral fuel slosh model was used in this investigation.

Several independent investigations have determined that lateral fuel sloshing behavior can be adequately represented by a pendulum analogy. The model consists of a fictitious pendulum mass suspended from a given point in each propellant tank to represent the sloshing liquid mass and a fictitious fixed mass in each tank to represent the nonsloshing mass. Generally, it is necessary only to simulate the fundamental mode of liquid sloshing, since higher-mode natural frequencies are much greater than attitude control frequencies, and since the lateral forces produced by the high modes are small. The model parameters for an unbaffled spheroidal tank are: (1) M_p, slosh mass, (2) M_o, nonslosh mass, (3) L_p, length of pendulum arm, (4) h_p, distance from center of tank to pendulum hinge point, (5) h_o, distance from center of tank to fixed mass, and (6) ξ, pendulum damping. The values for these parameters have been empirically determined and are functions of the liquid depth and viscosity, and of tank size.

Figure 5-2 is an illustration of the model and parameter values for half-full tanks of N_2O_4 and MMH. Half-filled tanks were used in the simulation, since the lateral forces are maximum at that depth. Because the tanks were to be rotating off their centers in a three-dimensional simulation, it was felt that the model would be more representative if 2-degree-of-freedom or conical pendulums were used. However, because we are now dealing with rotating reference frames, a component of coriolis acceleration, $2\bar{\omega} \times \bar{L}_p$, is present. But notice that in the model L_p is fixed, and thus $2\bar{\omega} \times \bar{L}_p = 0$, i.e., the coriolis component has been incorrectly zeroed out. Since coriolis acceleration is next to impossible to understand physically, one can only hope that the effect of coriolis acceleration on the fundamental mode behavior is insignificant. Whether this is true or not is yet to be determined.

D. NUTATION DAMPER

One of the simplest and most economical ways to reduce small nutation angles in spinning spacecraft is with a passive nutation damper. The major types being flown today are liquid-filled hoops or tubes and tuned pendulums. The effectiveness of a damper depends on how sharply resonant it is (i.e., the bandwidth) and on how close the damper resonant frequency is to the precession frequency. The bandwidth of the damper is a direct function of the damping constant ξ. Small values of ξ result in sharply resonant dampers that provide the most efficient nutation damping; however, should the precession frequency move slightly off the resonant frequency due to mass changes, the damper will become ineffectual. Hence, the bandwidth of the damper must be sufficient to cover the range of precessional frequencies over the life of the mission, or the damper must be tunable.

Liquid-filled dampers are viable only when mounted on the spin section, and hence their application is limited to vehicles with oblate inertia distributions. Unlike the pendulum type, they are typically high bandwidth with long time constants and operate over a wide range of precession frequencies. The principal advantages of a fluid damper

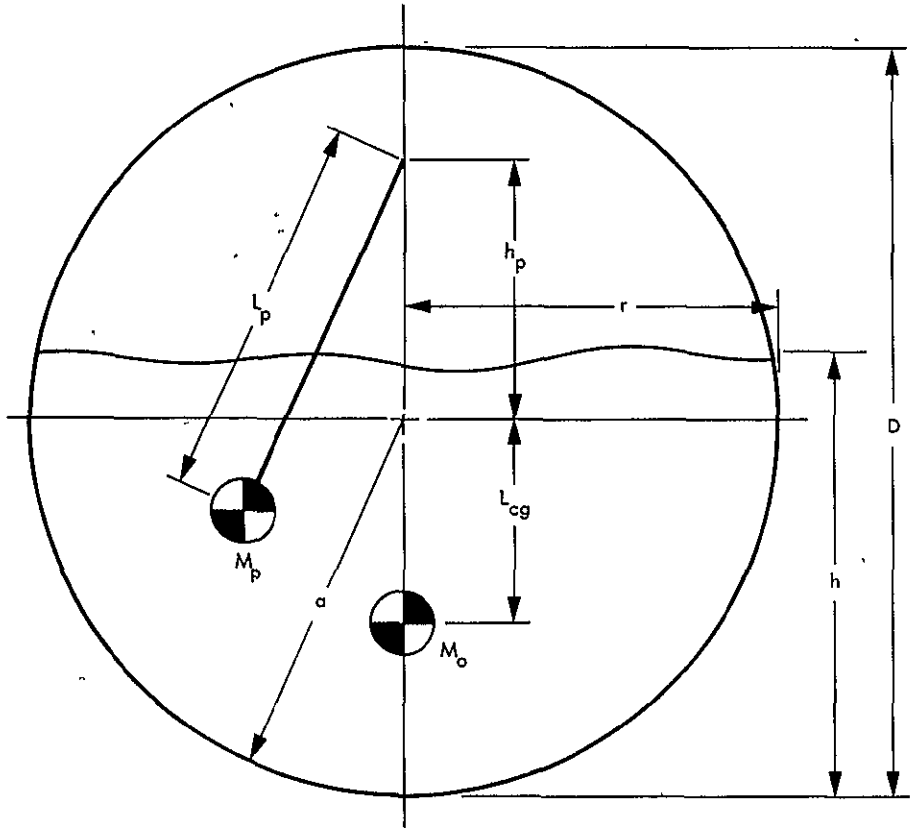

PARA \ FUEL	N_2O_4	MMH
M_o	44.517 kg	22.264 kg
M_p	56 661 kg	28.336 kg
h_p	0 0137 m	0.0137 m
L_p	0 2192 m	0 2192 m
L_{cg}	0	0
h/D	0.5	0.5
a,r	0 343 m	0.343 m
η	1.25	1.25
ω_N	0.9256 rad/s	0.9256 rad/s
g	0.1878 m/s^2	0 1878 m/s^2
ξ	0.017	0.026

Fig. 5-2. Conical Pendulum Fuel Slosh Model

over a pendulum damper, assuming an oblate spacecraft, are its simple construction, light weight, and low cost; for these reasons, it is considered a prime candidate for JOP. Fluid dampers are typically mounted off the bearing axis in a plane parallel to it. Placement of the damper is not critical, and as a result, it can additionally serve as a balance weight on the spin section to reduce ballast mass. Modeling of the liquid fluid damper is quite involved and limited at best because of the high nonlinearity of liquid behavior. For this reason, and because damper design was not of primary interest at this stage, a more easily modeled tuned pendulum damper mounted on the despin section was used in the simulation.

Tuned pendulum dampers take on several forms, but for small angles, the operating principles are the same and the choice is usually a matter of engineering convenience. A 2-degree-of-freedom spring pendulum with fluid damping of the type used on the Orbiting Solar Observatory (OSO) was selected for use in the simulation. The undamped natural frequency of a spring-mass pendulum free of gravitation is given by

$$\omega_{np} = \sqrt{\frac{K_p}{m_p L_p^2}} \tag{11}$$

where

ω_{np} = undamped natural frequency, rad/s

m_p = mass of the pendulum bob, kg

L_p = length of pendulum, m

K_p = spring constant, Nm/rad

The damper was designed to accommodate economic computer runs and is more massive than required for the actual JOP spacecraft. Its characteristics are:

$$\omega_{np} = 0.716 \text{ rad/s}$$

$$m_p = 5 \text{ kg}$$

$$L_p = 0.242 \text{ m}$$

$$K_p = 0.15 \text{ Nm/rad}$$

which results in a spacecraft damping time constant of 85 s. A bob mass of around 1 kg is a more reasonable choice for JOP, since spacecraft weight is critical. This would increase τ to 500 s, viz., it would take approximately 1/2 h for the precession to be completely damped. Although the bob mass is only 1 kg, the weight of the entire unit will most likely be unacceptable for JOP. For example, OSO had a bob mass of only 0.38 kg, and yet the damper unit weighed over 5 kg.

SECTION VI

ANALYSIS AND SIMULATION RESULTS

The principal objective of this study effort was to identify the fundamental stability and configuration limitations of a dual-spin JOP vehicle to insure that technically and economically realistic designs could be developed and implemented that would satisfy the JOP mission and attitude control requirements. Figure 6-1 shows a matrix of the sensitivities investigated. The columns of the matrix are those items that may affect the performance of the items listed in the rows. Asterisks indicate the sensitivities investigated. (Note that an asterisk does not necessarily represent a single computer run; it could be one, many, or part of another run.)

A. SCAN POINTING AND SLEWING

The scan pointing loops were designed to operate in the presence of precession and wobble. Scan sensitivities were obtained by comparing peak steady-state scan pointing errors as a function of bandwidth, boom flexibility, fuel slosh, and precession. A baseline simulation run was established with the following properties: rigid booms, no fuel slosh, clock and cone controller bandwidths of 0.4 and 1.5 Hz, respectively, and a constant precession at 0.7 rad/s with a nutation angle of 16.5 mrad. As one would expect, scan pointing errors decrease with increasing bandwidth. For a given bandwidth, the clock error will be larger than the cone error, since the inertia about clock is larger. The amount of difference is proportional to the ratio of the clock to cone inertias as seen by the control loops. In our case, this ratio is approximately 100. Scan pointing sensitivities to bandwidth are illustrated in Fig. 6-2. Note that the following results are for a linear system and therefore should be considered best-case. When fuel slosh was added to the baseline run, no appreciable sensitivity was experienced. On the other hand, boom flexibility proved to be significant; clock error was increased by a factor of 6.5, cone error by 11.

	SCAN CONTROL LOOP BW	FUEL SLOSH	FLEXIBLE BOOMS	SCAN SLEWING	A/C MANEUVER	ΔV MANEUVERS	SPIN RATE CONTROL	ω_P/ω_R
SCAN POINTING	*	*	*		*		*	
HGA POINTING/ ATTITUDE CONTROL		*	*	*		*	*	*
SPIN CONTROL		*	*					
WOBBLE CONTROL		*	*					
NUTATION DAMPING		*	*					

Fig. 6-1. Sensitivity Matrix

The next sensitivity investigated was the effect of scan slewing on spacecraft stability. Whenever the scan platform is torqued in clock or cone, momentum is transferred to the transverse axes and precession results. If the induced nutation angle exceeds the HGA pointing deadband, communications with the earth could be interrupted. Worse yet, if the torques are of sufficient strength and duration, instability could occur. Thus, the objective of this set of sensitivities was to first ascertain whether or not the spacecraft is stable during scan slewing and next, given that the system is stable, what slew rates and settling times can be achieved while maintaining the nutation angle at an acceptable level.

Nutation angle sensitivities were run as a function of scan clock rates and settling times. The system was considered settled after four time constants of the control loop, and the slew duration for each case was 15 s. The nominal spin rate was 5 rpm. Again, the system was linear except for the bearing actuator, which was torque-limited to ±2.82 Nm.

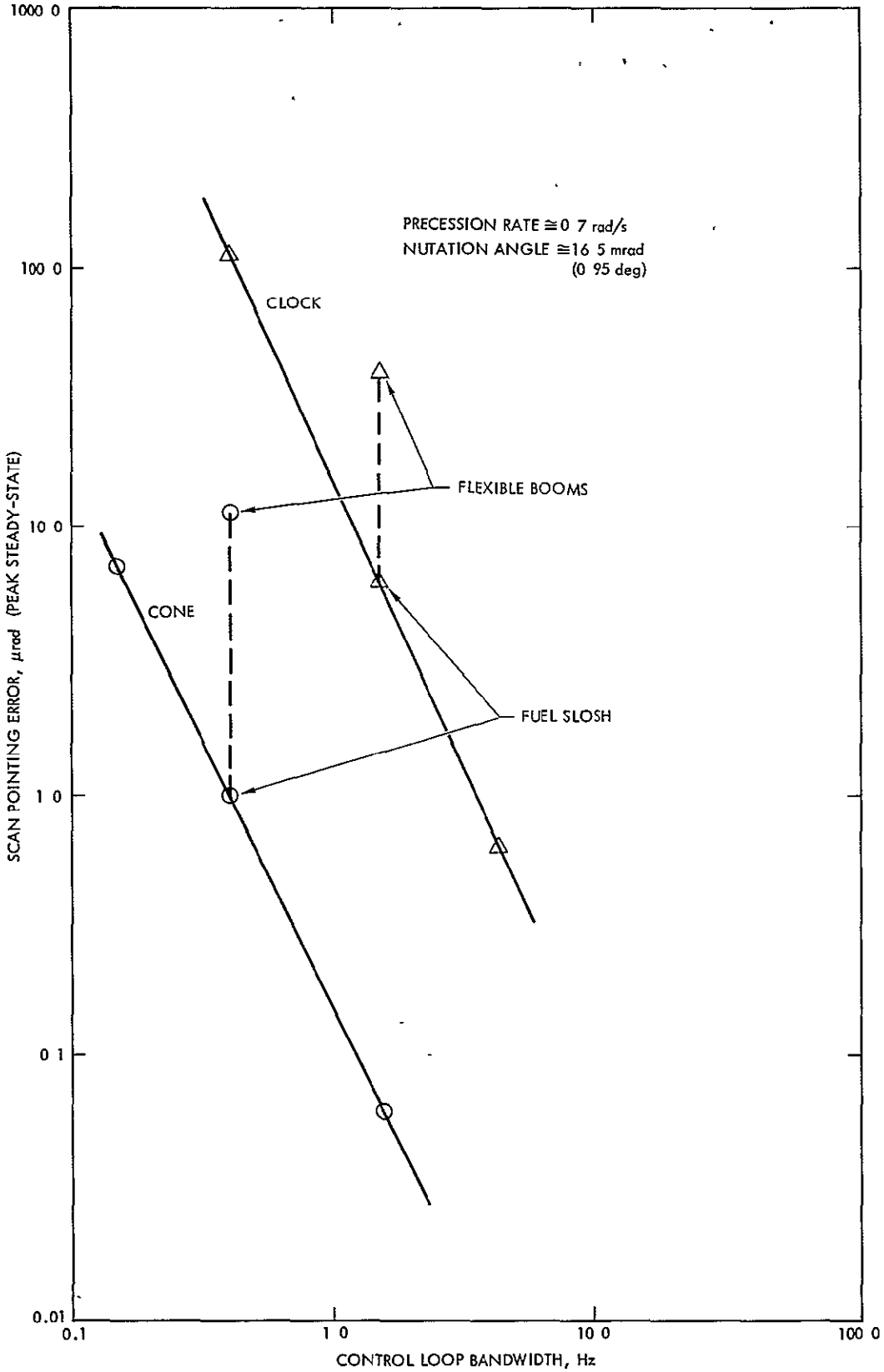

Fig. 6-2. Scan Pointing Sensitivities — Bandwidth, Flexible Booms, and Fuel Slosh

The initial goal for the scan slew rate was 2.0 deg/s, with a settling time of less than 8 s. The cone axis, because of the small inertias involved, had no difficulty meeting this goal. The resulting peak torque and induced nutation angle were quite small compared to those of the clock axis. Figure 6-3 presents the results of scan clock slew sensitivities. The ordinate represents the peak nutation angle experienced as a result of slew start-up or stopping transients. The actual peak nutation for complete slew maneuvers could be twice that shown in Fig. 6-3, since the induced nutation due to starting and stopping can be additive. The numbers above each test point represent the torque saturation time of the bearing actuator, or the peak torque required if saturation did not occur. For a 2-deg/s clock slew rate, the bearing actuator was in hard saturation over the entire range of acceptable settling times. Even if the actuator could have provided the required torque, the induced nutation angle would still have exceeded the HGA pointing deadband. Therefore, 2 deg/s is not a viable slew rate in clock for a spin rate of 5 rpm. The spin rate can be increased to lower the 2-deg/s curve below HGA deadband, but the torque problem still exists. Several runs were made with the torque unbounded; the peak torques experienced during the transients were on the order of 30-40 Nm. An actuator of this size is not only impractical from a power standpoint, but the size of the motor nonlinearities now starts to become significant. Reducing the slew rate to 1 deg/s helped considerably. For scan settling times greater than 1.5 s, the induced nutation angles are less than the HGA deadband, but the margin of safety is insufficient even at a settling time of 8 s. A safety margin of at least 50% is required if both starting and stopping transients are to be considered. The spin rate can be increased to 10 rpm to provide an adequate safety margin; or alternatively, a scan rate of 0.5 deg/s could be used if acceptable. Notice that increasing the settling time (decreasing the controller bandwidth) has little effect on the induced nutation; decreasing the slew rate does, however, have a significant effect. In fact, the induced nutation is reduced in direct proportion to the reduced slew rate.

The final scan sensitivity addressed was the effect of an attitude control or HGA pointing maneuver on scan pointing performance, viz.:

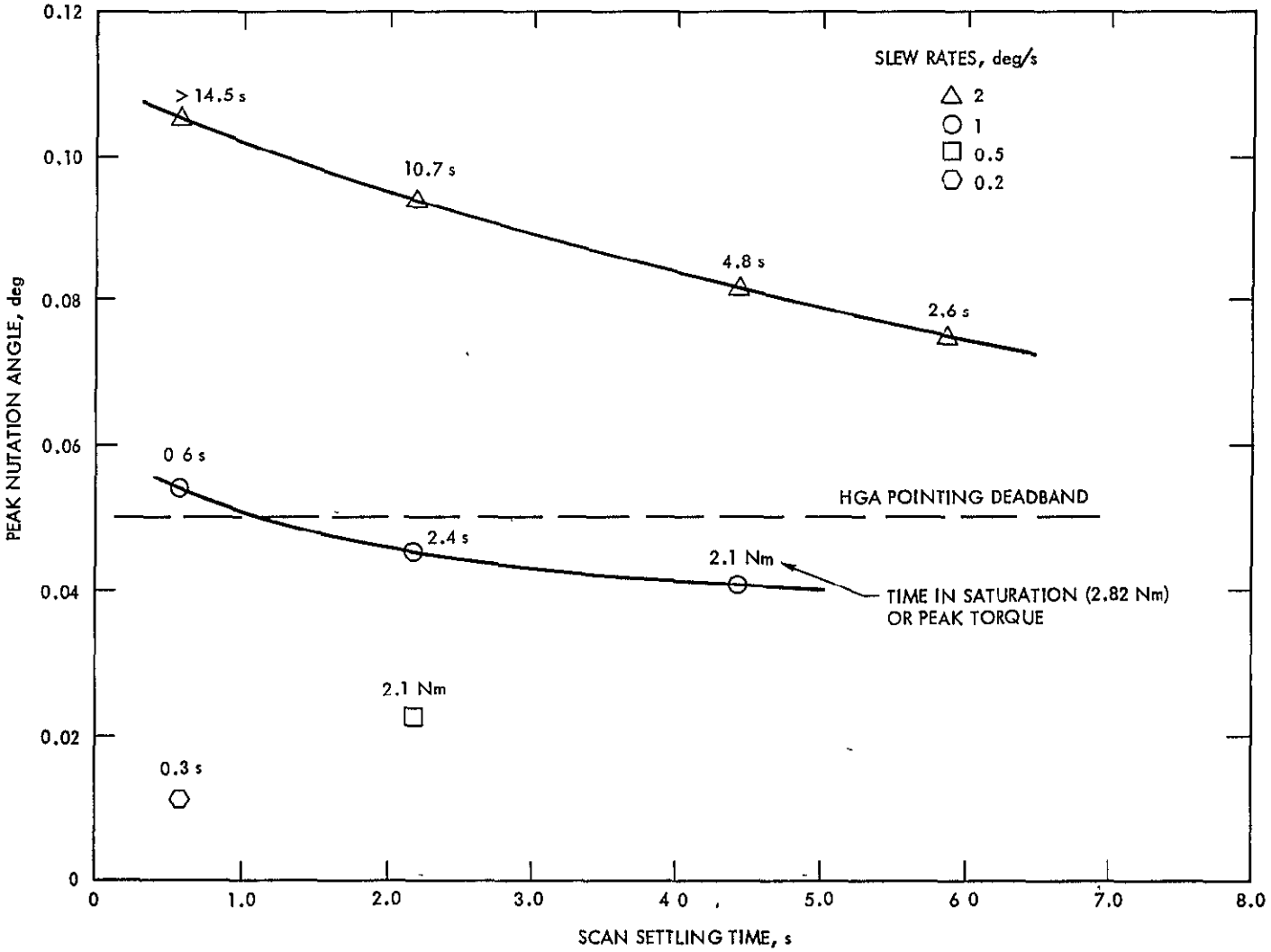

Fig. 6-3. Nutation Sensitivity to Scan Clock Slewing

Given that an attitude control maneuver occurs during an imaging sequence, what kind of scan pointing errors can be expected? The baseline run contained clock and cone control bandwidths of 1.5 and 0.4 Hz, respectively, rigid booms, no fuel slosh, and a 27.5-mrad attitude correction maneuver using the three-burn scheme. The maneuver is illustrated in Fig. 6-4. The resulting peak scan rates and positions for the baseline run, the baseline plus fuel slosh, and baseline plus flexible booms are presented in Table 6-1. The 24.7-mrad maneuver was selected to represent an exaggerated worst case. Obviously, an imaging sequence would not occur simultaneously with a maneuver of that size, i.e., the bearing axis would not be allowed to drift that far off the earthline before the attitude was corrected. A maneuver size on the order of 1 mrad, the HGA pointing deadband, would be more representative. The magnitudes of the rates and positions for a maneuver of this size would be approximately 1/25 of those listed in Table 6-1. From these results, it is reasonable to assume that HGA pointing correction maneuvers occurring during science imaging will not appreciably affect imaging quality.

B. HIGH-GAIN ANTENNA POINTING

High-gain antenna pointing can be equivalently thought of as attitude control. The very process of HGA pointing maintains the attitude of the spacecraft, since the HGA is rigidly attached to it. The primary internal disturbance sources for HGA pointing are scan platform slewing and spin rate correction maneuvers.

As seen in the previous section, scan slew maneuvers can significantly affect the position of the bearing axis. Scan slew rates must be kept sufficiently small so as not to induce nutation comparable in size to the HGA pointing deadband. Previous results indicate that the maximum acceptable clock slew rate will be on the order of 0.5 deg/s for a spin rate of 5 rpm. Cone slew rates can be any practical value, since cone slewing has little effect on HGA pointing performance.

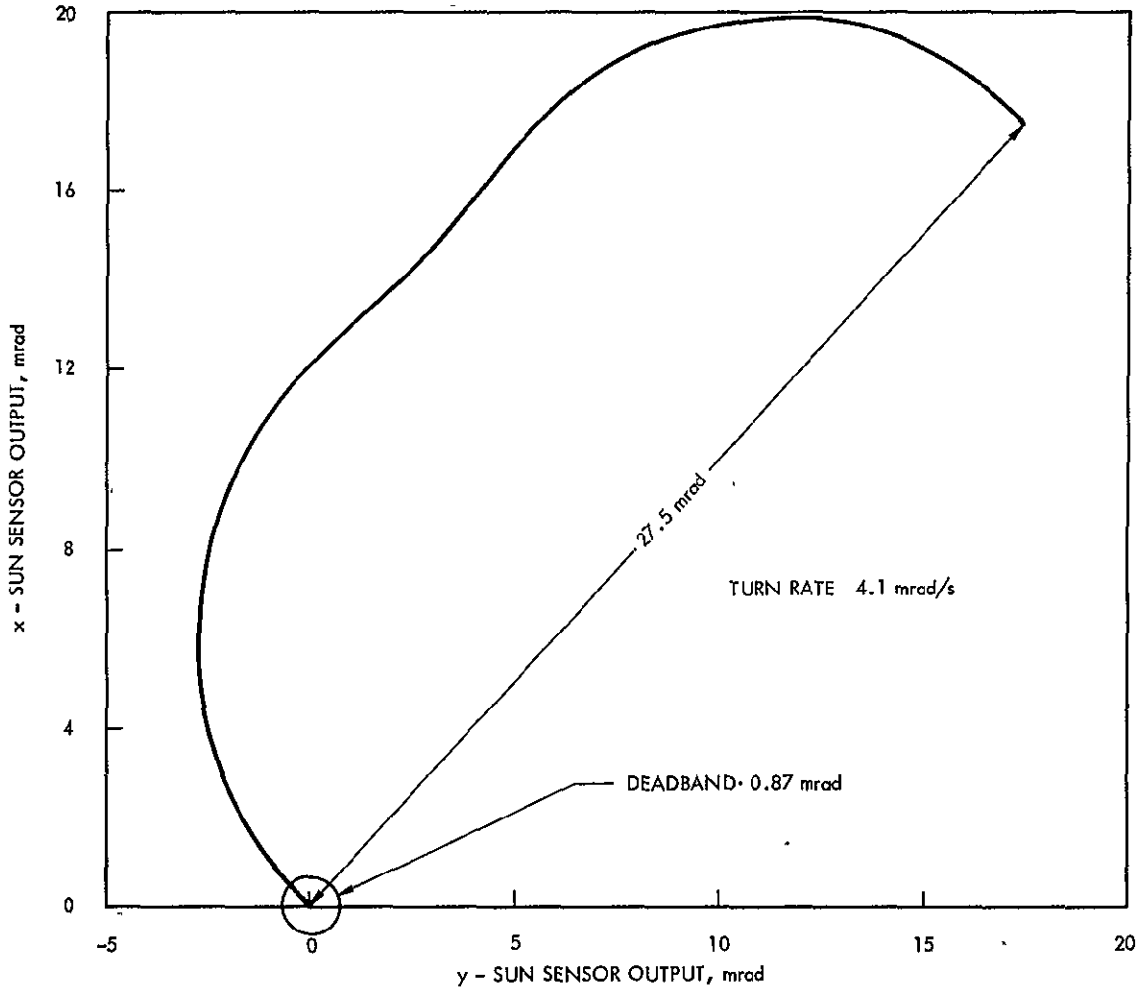

Fig. 6-4. Attitude Control Maneuver — Three-Burn Scheme

Table 6-1. Scan Pointing Sensitivity to Attitude Control Thruster Firings

Scan Pointing Errors (Peak) / A/C Sensitivity	Cone Angle		Clock Angle	
	Position, μrad	Rate, μrad/s	Position, μrad	Rate, μrad/s
Baseline run Cone BW = 0.4 Hz Clock BW = 1.5 Hz Correction = 24.7 mrad	0.55	0.59	6.5	27.0
Baseline + flexible booms	0.68	0.47	10.0	55.8
Baseline + fuel slosh	0.64	0.57	8.5	28.7

Spin rate control performance sensitivity runs show that for a 4% spin rate correction with flexible booms, the amount of induced nutation is comparable to the HGA deadband. Since the spin rate control deadband is expected to be 5-10% of the nominal spin rate, spin rate correction maneuvers will have to be performed in increments of 2% or so to insure accurate HGA pointing. This sensitivity should be reexamined as the boom design becomes final and better flexibility models are available. Spin rate corrections in the presence of fuel slosh had no appreciable effect on HGA pointing performance.

The accuracy of attitude correction maneuvers depends on many things. One of the early questions was the sensitivity of precession maneuvers to fuel slosh and boom flexibility. Figure 6-5 shows the results of attitude correction maneuvers for a rigid spacecraft, for a spacecraft with fuel slosh, and for a spacecraft with flexible booms. When comparing the rigid to the nonrigid body cases, it is concluded that flexible booms and fuel slosh will probably not impair attitude correction maneuvers. This conclusion is qualified because the fuel slosh model is questionable and only the fundamental mode of flexibility was used. As the spacecraft configuration firms up and better models are available, another look at this sensitivity would be appropriate.

Notice in Fig. 6-5 that there is residual nutation at the end of the maneuver, and that it is comparable in size to the HGA pointing deadband of 0.87 mrad. This occurred because the estimated value of the precession rate was not equal to the actual precession rate of the vehicle. How accurately the precession rate must be estimated depends on the size of the maneuver, the type of burn scheme used, and the acceptable size of the residual nutation angle. The degree of accuracy required is illustrated by the following example. A 1-deg correction maneuver with a residual nutation angle of less than 10% of the HGA pointing deadband is desired. Assuming perfect thrusters and an exact estimate of the spin rate, the two-burn scheme requires knowledge of the precession rate to within 0.02%. The three-burn scheme requires about 0.4%. As the size of the maneuver is decreased, the accuracy

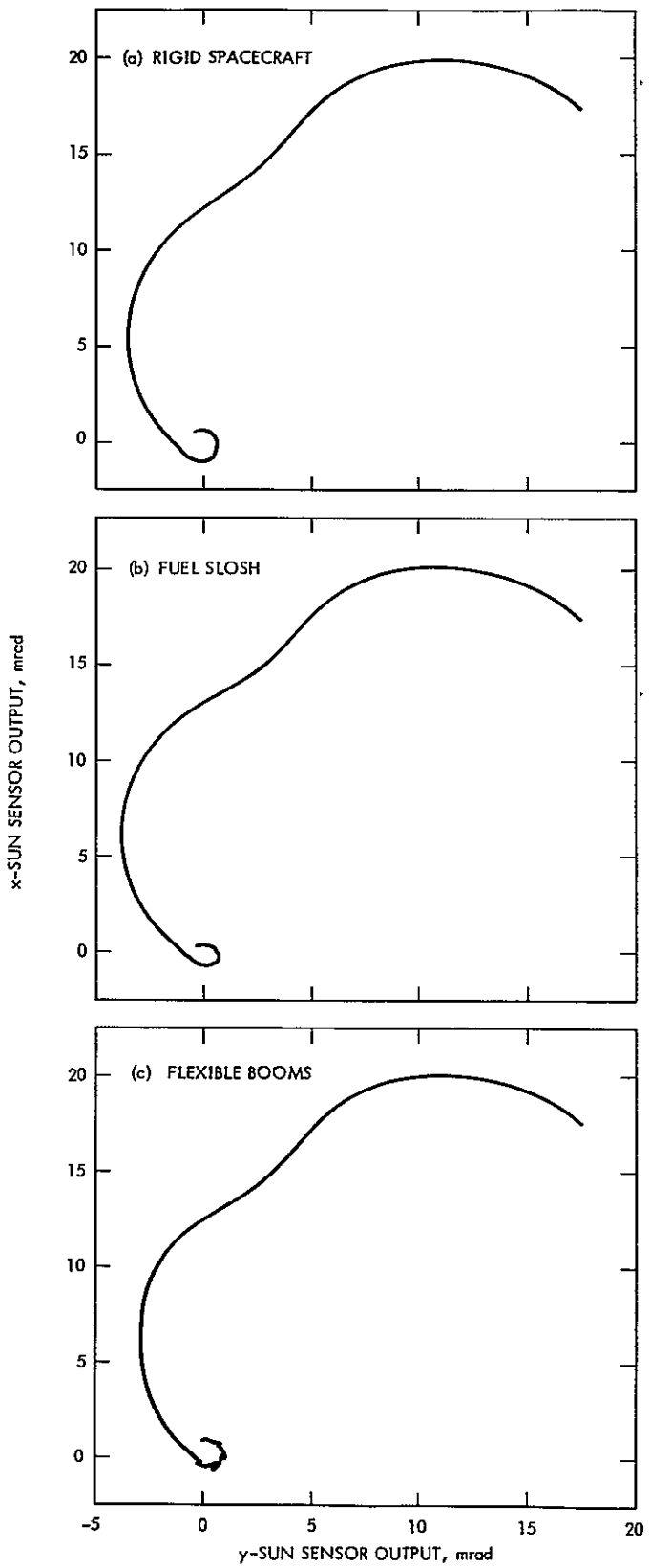

Fig. 6-5. Attitude Control Sensitivity to Fuel Slosh, Flexible Booms, and Knowledge of Precession Rate

requirements also decrease. For a 0.1-deg correction, the required accuracies are 0.2% and 4% for the two- and three-burn schemes, respectively.

Other items that may affect the accuracy of attitude correction maneuvers are thruster pulse shape, accuracy of spin rate estimate, spin/despin encoder resolution, quantization effects, and, of course, the accuracy of the attitude sensors. Cursory analysis indicates that these items should not significantly affect the accuracy of the attitude correction maneuvers. They should be reexamined, however, once the final spacecraft and attitude control configuration are decided upon.

C. NUTATION DAMPING

The damper was designed to operate at a precession frequency of 0.7 rad/s, with a nutation damping time constant of 85 s. A rigid baseline run was set up and the desired performance achieved.

When fuel slosh was added, the damping time constant unexpectedly increased approximately 5%. A possible explanation for this is the change in precession frequency away from damper resonance caused by a changing inertia ratio due to sloshing fuel. One would normally expect fuel slosh to aid the nutation damping, but because the natural frequency of the fuel slosh is 0.93 rad/s, with a very low damping constant, it is sharply resonant off the precession frequency, and hence, little damping occurred. The natural frequency of the fuel slosh will decrease as the fuel is depleted; thus, as the mission progresses, the amount of nutation damping from the fuel is expected to increase. Although some nutation damping from fuel can be expected, it can not be considered as a primary source of damping because of its variable behavior. A nutation damper either on the spin or despin section is required.

When the flexible booms were added to the baseline run, the damping behavior was essentially unchanged. This was expected, since

the natural frequency of the booms is well above the precession frequency. The booms can be designed to additionally serve as nutation dampers. An example of this is the bellows/magnetometer boom damper used on Pioneer. Damping with booms, however, does not appear to have any real advantage over the simpler dampers.

D. WOBBLE CONTROL

Neither fuel slosh nor flexible booms affected wobble angle control performance. Moving the RTGs to eliminate wobble naturally excites the booms, but their motion quickly dampens.

E. ΔV MANEUVERS

If the unbalanced despin section remains despun ($\omega_p = 0$) during a long ΔV maneuver in the direction of the bearing axis, such as Jupiter orbit insertion (JOI), $\bar{H}$ will continuously diverge due to a constant transverse torque T_t in the direction of the imbalance. However, if $\omega_p > 0$, T_t will be made to rotate in the x-y plane and will be averaged to zero. What effect T_t then has on the spacecraft attitude depends on ω_p; i.e., the larger ω_p, the faster T_t is averaged to zero. To study spacecraft attitude behavior in the presence of large ΔV maneuvers, a baseline simulation was set up as follows: $\omega_R = 5$ rpm, rigid booms, no fuel slosh, $\Delta V = 400$ N in the -z direction, and $\Delta t = 300$ s (burn time). Several runs were then made for various values of ω_p. When $\omega_p = 0$, $\bar{H}$ continuously diverged as expected. For $0 < \omega_p \leq \omega_R$, the peak excursion experienced by $\bar{H}$ decreased as ω_p/ω_R approached 1 and reached a minimum of 54 mrad when $\omega_p = \omega_R$, i.e., a single spinner.

Given the motion of $\bar{H}$ in inertial space, the other important variable to characterize is the nutation angle. When $\omega_p = 0$, the peak nutation angle as $\bar{H}$ diverged was 50 mrad. As ω_p was increased, a very interesting phenomenon occurred: at $\omega_p/\omega_R = 0.55$, the nutation angle went to infinity even though the motion of $\bar{H}$ was bounded in inertial space. When $0.5533 < \omega_p/\omega_R \leq 1$, the peak nutation angle again reduced to finite values and achieved a minimum of 95 mrad at $\omega_p/\omega_R = 0.8$.

Figure 6-6 shows plots of the peak angular deviations of the bearing axis, the angular momentum vector H, and the nutation angle as a function of $\omega_{p/R}$. Minimum bearing axis deviation occurs when the vehicle is a single spinner; however, the size of the deviation is still quite large -- 0.16 rad. The amount of deviation experienced is a function of the c.m. offset in the despin platform. For this particular configuration, the offset is large (20 cm) because the scan platform is mounted off to the side of despin platform and no endeavor is made to counterbalance it. Since angular deviations will also occur from imperfect thruster alignment, the despin platform should be balanced to minimize the effect on bearing axis deviation. Balancing within a centimeter would appear to be adequate for this configuration.

The nutation resonance experienced when $\omega_p/\omega_R = 0.55$ occurred as a result of asymmetry in spin section and cross products of inertia in the despin section. Given this type of inertia distribution, a dual-spin spacecraft will experience instability when $\omega_R - \omega_p = 0.5\ \lambda$, i.e., when the relative spin rate between the spin and despin section is equal to one-half the precession rate as seen by the despin platform. The value of ω_p/ω_R at which resonance occurs can be approximated by the following expression:

$$\omega_{p/R} \cong \frac{2I_t - I_R}{I_t + I_p} \tag{12}$$

For our configuration $\omega_{p/R} = 0.5533$ rad/sec, which is verified in Fig. 6-6. Notice that $\omega_{p/R}$ is not a function of thrusting; instability will be experienced in a dual spinner whenever it has asymmetry in the spin section, cross products of inertia in the despin section, and a relative spin rate between the spin and despin sections equal to one-half the precession rate as seen on the despin section. Thus, whenever the despin section is being spun up or spun down, the despin actuator must be able to provide sufficient torque to escape the resonance

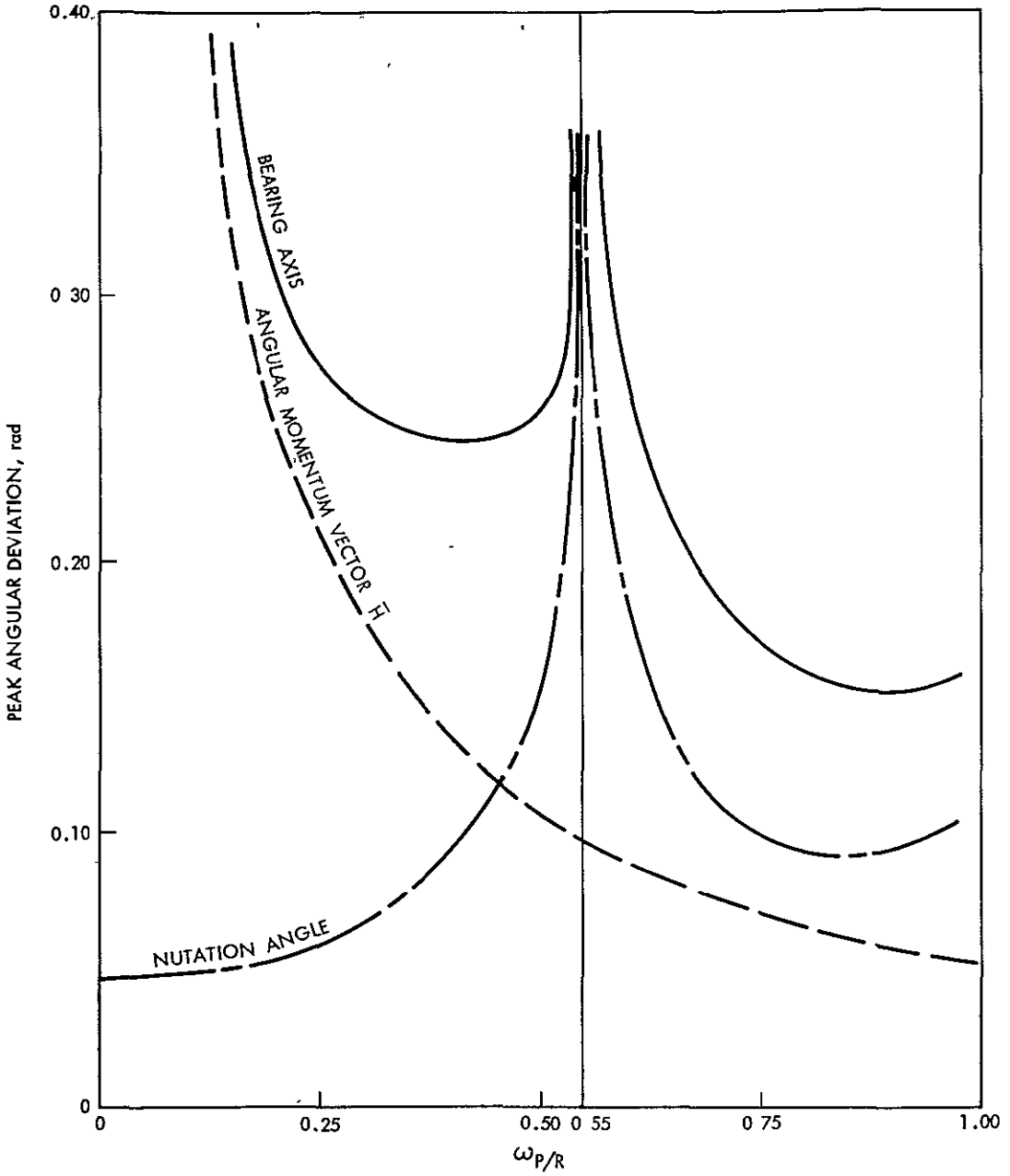

Fig. 6-6. Bearing Axis Deviation for Large ΔVs

region. If not, the platform rate can be captured, and the applied torque is then contributing to nutation buildup rather than to changing the platform rate. Determination of torque boundaries for capture in resonance is complicated by the time-varying nature of the problem. Simulation is the most straightforward means of establishing bounds for motor torque and mass asymmetries in a particular case to ensure passage through resonance. The baseline simulation was set up to slew the platform through $\omega_{p/R}$ at several different rates. Results show that the minimum torque required to escape resonance is well within the torque capability of the bearing actuator.

SECTION VII

SUMMARY

The applicability of dual-spin technology for a JOP mission has been investigated and verified. Preliminary mechanization and control concepts were developed, and key sensitivities and constraints identified using a comprehensive digital simulation.

Scan platform pointing performance proved to be sensitive to boom flexibility; effects due to fuel slosh, attitude correction maneuvers, and spin rate control maneuvers were negligible. Scan sensitivity to boom flexibility could be significant; therefore, every endeavor should be made to make the booms as stiff as possible so as not to unnecessarily restrict the control loop bandwidths due to structural resonances. Torsional modes of flexibility were not included in this investigation but should be considered once boom definition is sufficient.

High-gain antenna pointing was most sensitive to scan clock slewing and spin rate correction maneuvers. Ultimate scan slewing capabilities will be determined by the final despin platform inertia properties. It is desirable to keep the platform symmetric, with no cross products of inertia. Decreasing the inertia about the spin axis will also improve scan clock pointing performance and reduce bearing actuator power requirements.

Attitude correction maneuvers are moderately affected by fuel slosh and boom flexibility. Further analysis is required before a quantitative sensitivity can be determined. The accuracy of attitude control maneuvers depends on the knowledge of the spin rate and precession frequency. Knowledge to within 1% appears to be adequate. Vehicle attitude during large ΔV maneuvers is sensitive to mass imbalances in the spin and despin sections, and also to thruster imbalances for multi-engine propulsion systems. To insure attitude

stability, the bearing actuator must have sufficient torque to drive the despin platform through the nutation resonance.

All the sensitivities obtained in this study are a function of the vehicle mass and inertia properties. It will be necessary to reexamine them in greater depth once the spacecraft configuration takes final form. Particular attention should be payed to developing more complete fuel slosh, flexible boom, sensor, and actuator models. The mechanization concepts will also have to be reconsidered as the configuration changes.

Dual spinners have been successfully flown since the early 1970s in earth orbiting applications, both commercial and military. Although they have never been used for deep space exploration, there are no fundamental reasons not to do so. In early 1978, the Pioneer Venus spacecraft will be the first dual spinner to fly into deep space. In 1981, JOP will be the second, and it will be the first deep space explorer launched from the Space Shuttle.

APPENDIX A

BIBLIOGRAPHY

DYNAMICS AND CONTROL

1. G. J. Adams, "Dual Spin Spacecraft Dynamics Under Conditions of Rotating Unbalanced Platform and Rotor Assembly," XXVII Congress International Astronautical Federation, Anaheim, Ca., October 1976.

2. P. W. Cheng, et al; "Kalman Estimation and Control of Dual Spin Satellites," IEEE Trans. Aerospace and Electronics System, Vol. AES-13, No. 3, May 1977.

3. J. E. Cochran, "Nonlinear Resonances in the Attitude Motion of Dual Spin Spacecraft," AIAA Paper 76-787, AIAA/AAS Astrodynamics Conference, San Diego, Ca., August 18-20, 1976.

4. W. J. Dixon, "Attitude Perturbations of a Spinning Jupiter Orbiter Spacecraft," AIAA Paper 72-920, AIAA/AAS Astrodynamics Conference, Palo Alto, Ca., September 11-12, 1972.

5. A. H. Gale and P. W. Likins, "Influence of Flexible Appendages on Dual Spin Spacecraft Dynamics and Control," J. Spacecraft, Vol. 7, No. 9, September 1970.

6. P. S. Goel and N. K. Malik, "Active Stabilization of a Dual Spin Spacecraft Using Unbalance," J. Spacecraft, Vol. 12, No. 12, December 1975.

7. L. H. Grasshoff, "An Onboard, Closed-Loop, Nutation Control System for a Spin-Stabilized Spacecraft," J. Spacecraft, Vol. 5, No. 5, May 1968.

8. P. W. Likins, "Attitude Stability Criteria for a Dual Spin Spacecraft," J. Spacecraft, Vol. 4, No. 12, December 1967.

9. J. E. McIntyre and M. J. Gianelli, "Bearing Axis Wobble for a Dual Spin Vehicle," J. Spacecraft, Vol. 8, No. 9, September 1971.

10. D. L. Mingori, et al., "Constant and Variable Amplitude Limit Cycles in Dual Spin Spacecraft," J. Spacecraft, Vol. 9, No. 11, November 1972.

11. B. O. Lange, et al., "Control Synthesis for Spinning Aerospace Vehicles," J. Spacecraft, Vol. 4, No. 2, February 1967.

12. K. R. Lorell and B. O. Lange, "An Automatic Mass-Trim System for Spinning Spacecraft," AIAA Journal, Vol. 10, No. 8, August 1972.

13. K. J. Phillips, "Linearization of the Closed-Loop Dynamics of a Dual Spin Spacecraft," J. Spacecraft, Vol. 8, No. 9, September 1971.

14. M. P. Scher and R. L. Farrenkopf, "Dynamic Trap States of Dual Spin Spacecraft," AIAA Journal, Vol. 12, No. 12, December 1974.

15. L. Slafer and H. Marbach, "Active Control of the Dynamics of a Dual Spin Spacecraft," J. Spacecraft, Vol. 12, No. 5, May 1975.

16. J. W. Smay and L. I. Slafer, "Dual Spin Spacecraft Stabilization Using Nutation Feedback and Inertia Coupling," J. Spacecraft, Vol. 13, No. 11, November 1976.

17. M. P. Scher, "Effects of Flexibility in the Bearing Assemblies of Dual Spin Spacecraft," AIAA Paper No. 70-1043, AAS/AIAA Astrodynamics Conference, Santa Barbara, Ca., August 19-21, 1970.

18. G. T. Tseng and K. J. Phillips, "Attitude Stability of a Flexible, Dual Spin Spacecraft with Active Nutation Damping Using Cross Products of Inertia," J. Astronautical Sciences, Vol. XXIV, No. 3, July-September 1976.

19. K. Tsuchiya and H. Saito, "Dynamics of a Spin-Stabilized Satellite Having Flexible Appendages", AIAA Journal, Vol. 12, No. 4, April 1974.

20. N. H. Wright, "Wobble Correction for a Dual Spin Vehicle," J. Spacecraft, Vol. 11, No. 4, April 1974.

STABILITY

21. K. T. Alfriend, "Stability of a Dual Spin Satellite with Two Dampers," J. Spacecraft, Vol. 11, No. 7, July 1974.

22. D. L. Mingori, "Effects of Energy Dissipation on the Attitude Stability of Dual-Spin Satellites," AIAA Journal, Vol. 7, No. 1, January 1969.

23. R. Sellappan and P. M. Bainum, "Motion of Spinning Spacecraft with Hinged Appendages," AIAA Journal, Vol. 15, No. 6, June 1977.

24. A. K. Sen, "The Dynamic Stability of a Dual Spin Satellite," IEEE Trans. Aerospace and Electronic Systems, Vol. AES-13, No. 4, July 1977.

25. T. M. Spencer, "Energy-Sink Analysis for Asymmetric Dual Spin Spacecraft," J. Spacecraft, Vol. 11, No. 7, July 1974.

26. G. T. Tseng, "Nutational Stability of an Asymmetric Dual Spin Spacecraft," J. Spacecraft, Vol. 13, No. 2, February 1976.

NUTATION DAMPERS

27. J. C. Amieux and A. Liegeois, "Design and Ground Test of a Pendulum-Type Active Damper," J. Spacecraft, Vol. 11, No. 11, November 1974.

28. G. A. Haines and C. T. Leondes, "Eddy Current Nutation Dampers for Dual Spin Satellites," J. Astronautical Sciences, Vol. XXI, No. 1, July-August 1973.

29. J. T. Neer, "INTELSAT IV Nutation Dynamics," AIAA Paper No. 72-537, AIAA 4th Communications Satellite Systems Conference, Washington D.C., April 24-26, 1972.

30. K. Phillips, "Active Nutation Damping Utilizing Spacecraft Mass Properties," IEEE Trans. Aerospace and Electronic Systems, Vol. Aes-9, No. 5, September 1973.

31. C. C. Schneider, Jr., and P. W. Likins, "Nutation Dampers vs Precession Dampers for Asymmetric Spinning Spacecraft," J. Spacecraft, Vol. 10, No. 3, March 1973.

FUEL SLOSH

32. H. N. Abramson, The Dynamics Behavior of Liquids in Moving Containers, NASA SP-106, 1966.

33. R. C. Michelini and R. S. Ghigliazza, "The Motion of Fluids in Spinning Crafts and Its Influence Upon Attitude Stability," 5th IFAC Symposium on Automatic Control in Space, Genoa, June 4-8, 1973.

34. E. R. Martin, "Experimental Investigations of the Fuel Slosh of Dual Spin Spacecraft," COMSTAT Technical Review, Vol. 1, No. 1, Fall 1971.

35. I. E. Sumner, Experimentally Determined Pendulum Analogy of Liquid Sloshing in Sphere and Oblate-Spheroidal Tanks, NASA TND-2737, 1965.

MISCELLANEOUS

37. C. Edgcombe, and J. A. Holt, "The Hybrid Simulation of a Dual Spin Spacecraft," International Seminar, Simulation and Space, Toulouse, September 10-14, 1973.

38. D. L. Mackeson and R. L. Gutshall, "Star Scanner Attitude Determination for the OSO-7 Spacecraft," J. Spacecraft, Vol. 10, No. 4, April 1973.

39. D. L. Mackison and R. L. Gutshall, "OSO-7 Spacecraft Star Scanner System Accuracy," AIAA 11th Aerospace Sciences Meeting, Washington D.C., January 1973.

40. F. F. Mabley, et al., "The Attitude Control and Determination Systems of the SAS-A Satellite," APL Technical Digest, June 1971.

41. J. M. Wilson and D. E. Maas, "Three-Axis Air Bearing Test Results of a Dual-Spin Spacecraft," AIAA Paper No. 72-860, AIAA Guidance and Control Conference, Stanford, Ca., August 11-16, 1972.

42. Proceeding of the Symposium on Attitude Stabilization and Control of Dual-Spin Spacecraft, Aerospace Corporation, El Segundo, Ca., August 1-2, 1967.

43. G. E. Fleischer and P. W. Likins, Attitude Dynamics Simulation Subroutines for Systems of Hinge-Connected Rigid Bodies with Nonrigid Appendages," TR 32-1598, Jet Propulsion Laboratory, Pasadena, Ca., August 1975.

44. M.H. Kaplan, Modern Spacecraft Dynamics and Control, John Wiley and Sons, New York, 1976.

APPENDIX B

JOP MASS AND INERTIA PROPERTIES

Description	Mass (kg)	$\bar{x}$ (cm)	$\bar{y}$ (cm)	$\bar{z}$ (cm)	I_{xx},	I_{yy},	I_{zz}, kg m^2	I_{xy},	I_{xz},	I_{yz},
Despun platform	160	5.05	- 32.1	-139.8	139	111	151	10.21	1.95	-15.69
Scan platform	32	0	113.0	-116.8	1.19	1.84	2.66	0	0	0
Total despun section	192	4.20	- 7.74	-135.9	199	115	212	8.24	1.64	- 6.75
Total spin section, full fuel, probe	1097	-0.655	- 4.42	- 26.84	780	891	1512	-1.03	-1.36	-10.42
Total orbiter, full fuel, probe	1289	0.0677	- 4.91	- 43.08	1174	1200	1724	6.95	-8.37	-11.25
Total spin section, no fuel, no probe	341	-2.11	- 14.23	- 20.73	510	721	1180	-1.74	- .916	- 7.46
Total orbiter, no fuel, no probe	532	0.164	- 11.89	- 62.25	872	999	1393	7.01	8.21	-23.39

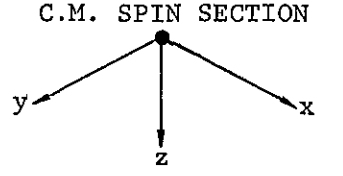

REFERENCE COORDINATES